JOURNAL OF CONDENSED MATTER NUCLEAR SCIENCE

Experiments and Methods in Cold Fusion

VOLUME 2, May 2009

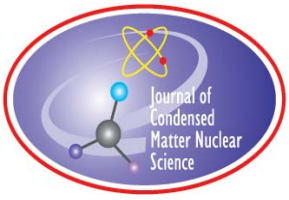

JOURNAL OF CONDENSED MATTER NUCLEAR SCIENCE

Experiments and Methods in Cold Fusion

JOURNAL OF CONDENSED MATTER NUCLEAR SCIENCE

Volume 2, May 2009

Orders, claims, author inquiries and journal inquiries

Please contact the Editor in Chief, CMNSEditor@iscmns.org or webmaster@iscmns.org

J. Condensed Matter Nucl. Sci. 2 (2009) 1–59

JOURNAL OF CONDENSED MATTER NUCLEAR SCIENCE

Volume 2 2009

CONTENTS

PREFACE

It is my pleasure to introduce the second volume of *The Journal of Condensed Matter Nuclear Science*. We are now 20 years after the birth of this new scientific field. More and more data prove that the effect is real and scientifically demonstrated. Gradually, the scientific community and the media at large are opening up to this reality. How much more time will be necessary in order to get full acceptance? Nobody knows. But we are on the correct trajectory.

This journal is a community one; the sort of journal found in any research field. It is destined to be read by specialists. It is the place where new data can be shown, and theories speculated upon. In this journal, we do not need to try to prove the existence of cold fusion in every article; we take it for granted that the effect is real. We bring data, observations or ideas: some are excellent and of great interest, others are less important. However, my 40 years of research experience have taught me that you never know at a given time what is important and what is not. A simple observation one day described in a paper may be important for someone else who has seen a similar fact, and never published it. A half-developed theory might give ideas to another theoretician to improve his own work.

The Journal of Condensed Matter Nuclear Science has two major difficulties hindering its growth. On one hand, it is tempting to publish good, solid data or theories in well-known refereed journals, which is quite understandable. On the other hand, almost every year there is an international conference and local workshops that help exchange information between scientists and allow publications in the proceedings of these meetings. Therefore, there is not much room for more papers to be published in *The Journal of Condensed Matter Nuclear Science*.

Interestingly, since we have an all electronics journal, we do not have the constraints of the printed ones. We basically have no page limitation, and it is very possible to publish here extended versions of papers published in proceedings, with the great advantage that it is an easily accessible journal, since downloading is free of charge.

I wish to thank the authors and the referees for their contributions.

Jean-Paul Biberian
May 2009

J. Condensed Matter Nucl. Sci. 2 (2009) 1–6

Research Article

Unexplained Explosion During an Electrolysis Experiment in an Open Cell Mass Flow Calorimeter

Jean-Paul Biberian *

Département de Physique, Faculté des Sciences de Luminy, Université d'Aix-Marseille, 163 Avenue de Luminy, 13288 Marseille Cedex 9, France

Abstract

While running an electrochemical cell designed to measure excess heat with a hollow palladium cathode and a platinum wire anode in heavy water, an explosion occurred. The Dewar that contained the experiment shattered. It is unlikely that the explosion was due to a deuterium oxygen recombination explosive reaction, since the cell was open, the amount of deuterium and oxygen gas was very limited in the cell and any pressure created by recombination should have escaped through the unsealed open end of the cell. It is very likely that under some not yet understood conditions, chain reactions occur in highly loaded palladium samples giving rise to an explosion. Several experimentalists before have already observed this same phenomenon.

Keywords: Cold fusion, LENR, CMNS, Excess heat, Explosion, Chain reaction

1. Introduction

Pons and Fleischmann [1,2] have shown that performing the electrolysis of heavy water in the presence of LiOD, with palladium cathode and platinum anode, excess enthalpy is observed that cannot be explained by normal chemical reactions. Later they worked on a cell that worked continuously in the boiling regime [3]. The idea of working at 100°C is coming from their observation that there is a positive feedback with temperature. The higher the temperature, the more excess heat was observed [4]. The experiment described in this paper has been designed to operate anywhere from room temperature to boiling with low input power. In the course of an experiment using a palladium tube as a cathode, an explosion occurred, and the whole cell got shattered into pieces. The conditions of the explosion cannot be explained by deuterium oxygen explosive recombination.

2. Experimental set up

The Pyrex electrolytic cell is a Dewar 50 cm long, 25 mm inner diameter, 40 mm outer diameter as shown in Fig. 1. Both Pyrex walls of the cell are 2.5 mm thick. The electrodes and the electrolyte are positioned in the bottom section.

*E-mail: jpbiberian@yahoo.fr

In the upper section, a coaxial water-cooled condenser 31cm in length, 22 mm in diameter absorbs the heat produced during electrolysis by condensing the water vapors due to the heat generated by electrolysis and also possible excess heat. Power output is calculated with the water mass flow circulating in the condenser and the difference between inlet and outlet temperatures. Temperatures are measured via two thermistors. The condenser is laying by its own weight on the upper part of the Dewar cell. It is not sealed.

The cathode is a 10 cm hollow palladium tube 2 mm outer diameter and 200 μm thick walls closed at the bottom, opened at the top. The anode is a 200 μm diameter platinum wire wrapped around the cathode. The electrolyte is 0.1 N LiOD in D_2O. The volume of electrolyte is at most 100 ml. In case the cell runs dry, this is also the maximum amount of D_2 and O_2 gases present in the cell and available for a chemical explosion.

Data are collected via a Labview software with a frequency of one set of data points every minute. Therefore, events occurring in a shorter time scale are not recorded.

The temperature of the electrolyte is not measured. The only thermal data available is the outlet temperature of the cooling device. The time constant of the heat measurement is about 10 min.

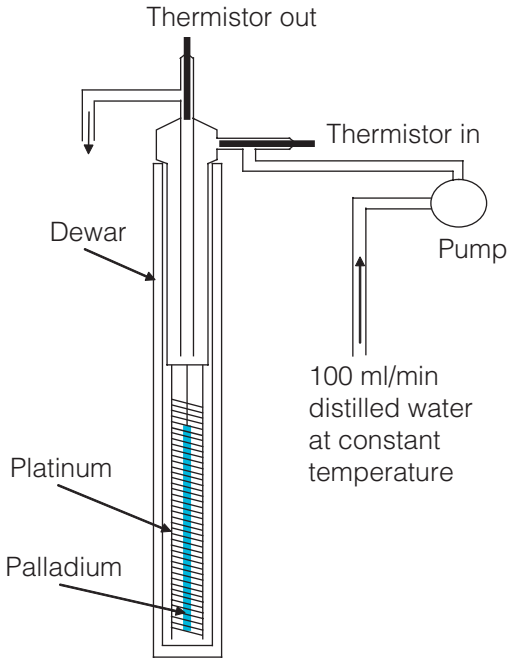

Figure 1. Schematic of the electrolytic cell.

3. Experimental results

The experiment lasted 30 days, and ended by the explosion of the cell. Figure 2 shows input and output power versus time.

In the first part of the experiment, the current applied is increased up to an input power of 34 W (3 A, 13.2 V). No excess heat is observed during this time period. Input power is then decreased and increased again with observation of

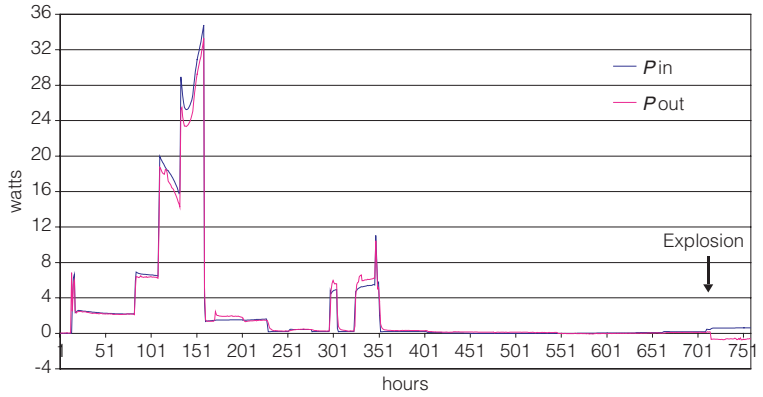

Figure 2. Power in and out (W) vs. time (h).

excess heat. Finally the input power is decreased and slowly increased again. However, when the explosion occurred, the current was only 0.2 A and 3.7 V. After the explosion the current remained the same, since the power supply was operating in constant current mode, however, the voltage increased to 4.5 V because there was still some electrolyte left at the bottom of the cell.

Figure 3 shows details of voltage and current at the time of the explosion. The explosion occurred 5 h after the current was raised from 0.1 to 0.2 A. The voltage increased with the current, then decreased steadily until the explosion. This is possibly an indication of a temperature rise in the cell, and probably simply correlated to the power increase inside the cell. There is no abnormal behavior in the voltage just before the explosion. It is no possible to know the exact level of electrolyte present in the cell at the time of the explosion, but probably low, knowing that no heavy water had been added in order to compensate for any loss by electrolysis.

Figure 4 shows the photographs of the cell and the Dewar before the explosion, and the condenser with the attached

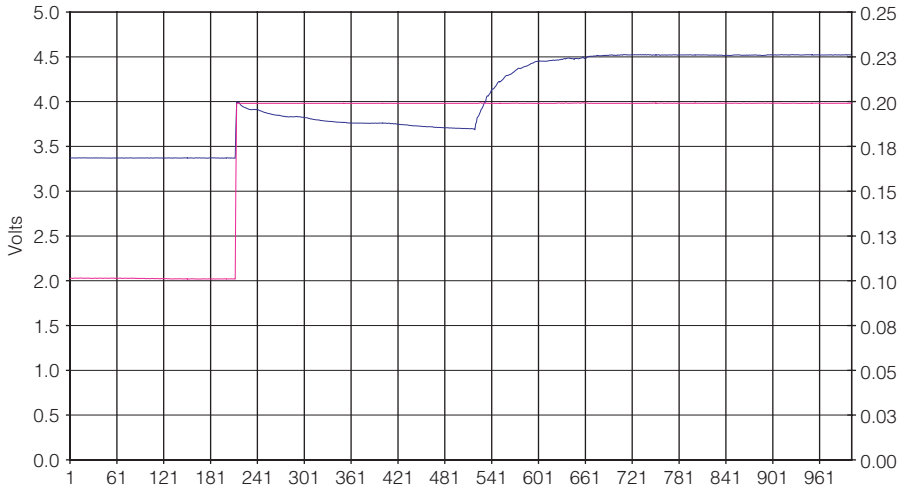

Figure 3. Details of voltage and current at the time of the explosion.

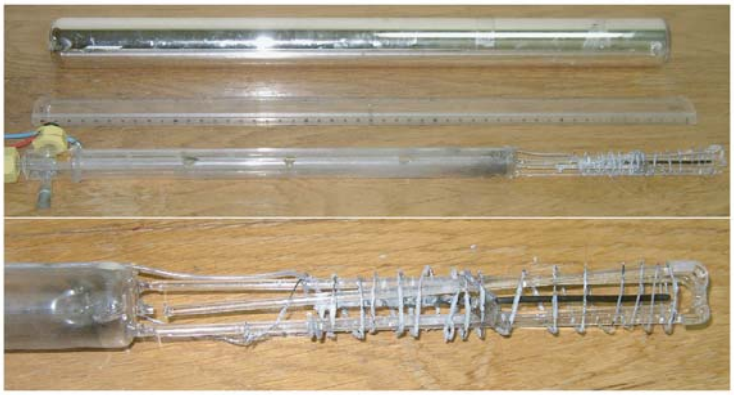

Figure 4. Top: a view of the Dewar. Bottom: views of the condenser and the cathode anode.

anode and cathode after the explosion. Figure 5 shows a picture of the remains of the Dewar after the explosion. As data points are acquired every minute, there was no indication of any change at the time of the explosion. Moreover, the cell temperature is not measured, only the water flow temperatures are monitored. The overall heat measurement time constant of the system being 10 min as mentioned above. Any sudden excess heat rise could not be detected.

Figure 5. Remains of the Dewar cell after the explosion.

It is very unlikely that the explosion was due to a deuterium oxygen recombination. As mentioned above, the amount of gases in the cell that could produce an explosion was only 100 ml. It is hard to believe that the Dewar will breakup by a recombination reaction knowing that the cell is not sealed.

In order to check the possibility of a violent recombination of deuterium and oxygen gas, an experiment was set up. A similar Dewar with similar electrodes was used. In addition a platinum wire was added on top of the cell where a current could be passed so that a gas explosion could be triggered. Electrolysis was performed long enough to make sure that there was no more air in the cell, and that only hydrogen and oxygen remained. The first test produced an explosion that raised the inner part of the cell by about 2 cm. The second experiment was performed in a similar fashion except that before triggering the explosion, the top of the cell was sealed with silicone glue. When the explosion was triggered, no damage was observed on the cell.

4. Conclusion

On several occasions, experimentalists have endured explosions. Pons and Fleischmann [5] have told that in one case, the palladium melted and fell down, producing damage on the concrete floor of their garage, Zhang et al. [6] using a hollow tube palladium cathode observed three explosions in an open cell. On January 2, 1992, an unfortunate explosion also occurred at SRI in a closed cell [7,8] that killed a scientist. The explosion was attributed to an oxygen deuterium violent recombination. More recently, 13 years later on the same day on January 2, 2005, Mizuno [9] experienced an explosion in an open cell that wounded him and deafened him and co-workers for several days.

These explosions seem to indicate that under certain circumstances, a sort of chain reaction is possible, and large quantities of heat are produced in a very short period of time. This type of behavior recalls heat bursts that are regularly observed during Cold Fusion experiments, and that are not reproducible. It seems that there are two regimes in Cold Fusion, one is steady at low level of excess heat, and the other one is fast and energetic.

References

[1] M. Fleischmann, S. Pons, M. Hawkins, *J. Electroanal. Chem.* **261** (1989) 301 and errata in Vol. 263.
[2] M. Fleischmann, S.Pons. M.W. Anderson. L.J. Li, M. Hawkins, *J. Electroanal. Chem.* **287** (1990) 293.
[3] S. Pons, M. Fleischmann, *Fourth International Conference on Cold Fusion,* 1993. Lahaina, Maui, 1993.
[4] S. Pons, M. Fleischmann, *J. Chim. Phys*. **93** (1996) 711.
[5] S. Pons, M. Fleischmann, Private Communication.
[6] X. Zhang, W.-S. Zhang, D. Wang, S. Chen, Y. Fu, D. Fan, W. Chen, *Third International Conference on Cold Fusion, "Frontiers of Cold Fusion"*. 1992. Nagoya, Japan, Universal Academy Press Inc., Tokyo, Japan.
[7] P.M. Grant, R.E. Whipple, F. Bazan, J.L. Brunik, K.M. Wong, R.E. Russo, B.D. Z. Andresen, *J. Radioanal. Nucl. Chem.* **193** (1995) 165–169.
[8] P.M. Grant, R.E. Whipple, A. Alcaraz, J.S. Haas, B.D.Z. Andresen, *Fusion Technol.* **25** (1994) 207–208.
[9] Report of the explosion at: http://www.newenergytimes.com/news/2005MTExplosion/2005MizunoT-AccidentReport.pdf

J. Condensed Matter Nucl. Sci. 2 (2009) 7–12

Research Article

4-Space Dirac Theory and LENR

A. B. Evans*

Department of Mathematics and Statistics, University of Otago, P.O. Box 56, Dunedin, New Zealand

Abstract

A 4-space Dirac theory, which gives the same transition energies as the standard model, predicts specific distributions of virtual electrons and positrons accompanying bound electrons. If potential barriers are viewed stochastically, it seems possible that this has implications for LENR.

Keywords: Stochastic barriers, Shielding, Dirac theory, Orbitals

1. Introduction

Those who seek a theoretical model for LENR face an immediate question. Does the explanation require an entirely new effect, lying outside currently accepted theory, or does it hinge on a hitherto overlooked consequence of the standard model? Given the complexities of the environments in which phenomena thought to be LENR are observed, the latter may seem more likely. Nevertheless, this paper presents an unconventional form of QED for the consideration of LENR researchers, in the hope that it may lead to theoretical progress.

Little-known versions of QED, known collectively as parametrized relativistic quantum theories [1,2], have for decades been investigated intermittently by researchers looking for models that clearly avoid any suggestion of a preferred frame of reference. In these models, the space-time coordinates $X^\lambda = (x^k, ct)$ are all on an equal footing, i.e. both spatial position and time are regarded as observables. An invariant parameter (called τ below), corresponding to the proper time of classical relativity, is used instead of t to describe the evolution of the wave function, which in the spin-$\frac{1}{2}$ theory proposed by the author [3] is a bispinor ψ satisfying a 4-space Dirac equation (Eq. (2)) that generalizes the conventional one.

As far as nonstandard QED is concerned, the first requirement is that its predictions must be extremely close – perhaps in many respects identical – to those of the standard model. For example, even a small departure from the energy levels of standard Dirac theory would immediately rule it out. Although the Dirac theory described below

*E-mail: bevans@maths.otago.ac.nz

allows solutions in which the proper mass m_0 - an observable in the 4-space formulation – is not sharp, it also gives stationary solutions – eigenstates of both energy and proper mass – that are formally identical to those of conventional Dirac theory, and imply the same transition energies. However, the 4-space solutions (including those for a Coulomb potential) generally require a modified interpretation of their wave functions, because the 4-space picture includes contributions from both electrons and positrons, as follows.

The invariant $\psi^\dagger(i\gamma^4)\psi \equiv F(\mathbf{X},\tau)$ is the expected space–time charge density, and the 4-vector $-\psi^\dagger\gamma^4\boldsymbol{\gamma}\psi \equiv \mathbf{J}(\mathbf{X},\tau)$ is the expected particle current, so that $J^4 = \psi^\dagger\psi \geq 0$ implies flow in the positive time direction. Thus $F = F_1 - F_2$, where F_1 and F_2 are electron and positron densities, and $\mathbf{J}$ is the sum of the particle and antiparticle currents, which are assumed to have a common 4-velocity $\mathbf{U}$ given by $c\mathbf{J} = (F_1 + F_2)\mathbf{U}$. A second invariant, $Q \equiv \psi^\dagger\gamma^0\psi$, where $\gamma^0 \equiv -i\gamma^1\gamma^2\gamma^3$, is related to F and $\mathbf{J}$ by $\mathbf{J}\cdot\mathbf{J} = -(F^2 + Q^2)$. It follows [3] that

$$F_1 = \left(\sqrt{F^2+Q^2} + F\right)/2,$$
$$F_2 = \left(\sqrt{F^2+Q^2} - F\right)/2. \tag{1}$$

The integrals of F_1 and F_2 over space–time do not generally represent whole numbers of charges, and we take this to mean that the expected 4-space densities may include contributions from virtual pairs, though usually at a very low level. We note that $F_2 = 0 \Leftrightarrow Q = 0$, and $F_1 = F_2 \Leftrightarrow F = 0$. We also find that F_1 and F_2 are interchanged by time reversal, as one might expect for electron and positron densities.

Later we use the Dirac representation, with its characteristic large and small components in a bound state: we then find that Q and (therefore) F_2 are normally small. However, in bound states Q increases with Z, giving rise to an increasing expected density of virtual pairs, and the model suggests pair creation when αZ is sufficiently close to 1. At the other extreme, a free particle has $Q = F_2 = 0$. Loosely speaking, Q measures the extent to which electromagnetic fields are producing virtual electrons and positrons - the effect increases with field strength. (Though as will be clear below, this does not mean that the electron and positron densities come separately from the large and small components of ψ.) Further details are given in [3,4], and the model has been illustrated by applying it to Klein's paradox [5].

2. Some General Results

The proposed 4-space Dirac equation is in general

$$\boldsymbol{\gamma}\cdot\left[\boldsymbol{\partial} - \left(\frac{ie}{\hbar c}\right)\boldsymbol{\Omega}\right]\psi = \left(\frac{i}{c}\right)\frac{\partial\psi}{\partial\tau}, \tag{2}$$

where the 4-component spinor ψ is a function of the space–time coordinates $X^\lambda = (x^k, ct)$ and the invariant parameter τ. Some of the conventions used here are those of [3]; in particular, the Lorentz metric tensor is $\eta_{\alpha\beta} = diag(1, 1, 1, -1)$. The chiral representation was used in [5], but the usual Dirac representation is better suited to the present purpose. In [3], m was used for proper mass, but m_0 is employed here.

The 4-space theory has a proper mass operator $\hat{m}_0 = (-i\hbar/c^2)\partial/\partial\tau$, and imposing the condition for sharp proper mass, $\hat{m}_0\psi = m_0\psi$, we reduce (2) to the conventional form

$$\boldsymbol{\gamma}\cdot\left[\boldsymbol{\partial}-\left(\frac{ie}{\hbar c}\right)\boldsymbol{\Omega}\right]\psi=-\left(\frac{m_0c}{\hbar}\right)\psi, \tag{3}$$

where $\psi=\mu(\mathbf{X})\mathrm{e}^{im_0c^2\tau/\hbar}$.

In the 4-space formulation, energy–time uncertainty is put on the same basis as that relating momentum and position, and so a particle that is not in an eigenstate of energy has a non-uniform distribution in time. On the other hand, eigenstates of proper mass give distributions that are independent of τ. To be realistic, therefore, eigenstates of proper mass must also be eigenstates of energy – otherwise we get a non-uniform distribution in time that does not move forward in time as τ increases. We therefore now suppose that

$$\psi=\nu(\mathbf{x})\mathrm{e}^{i(E_0\tau-Et)/\hbar}. \tag{4}$$

where ν depends only on the spatial coordinates x^k , as indicated.

In the Dirac representation, if ψ is split into 2-component spinors ξ and η, it is found that the fundamental invariants defined above are

$$F=\xi^\dagger\xi-\eta^\dagger\eta;\quad Q=\xi^\dagger\eta+\eta^\dagger\xi. \tag{5}$$

Adopting the usual convention that ξ and η are respectively the large and small parts of ψ, we can write $\eta\sim\alpha Z\xi$. Provided Z is not too large, we shall therefore have $Q\ll F$, so that the electron and positron densities in Eq. (1) give

$$F_1\approx F;\quad F_2\approx Q^2/4F. \tag{6}$$

But (5) gives space–time densities, whereas we want the expected spatial density of charge. A self-consistent formulation requires [5] that in stationary states the spatial density is FU^4/c , where $\mathbf{U}$ is the 4-velocity of a spatial frame in which the state is stationary. Hence the expected spatial charge density of a stationary 4-space model in its preferred reference frame is just $F(x)$. However, this in general is different from the usual expected charge density, which is

$$J^4=\psi^\dagger\psi=\xi^\dagger\xi+\eta^\dagger\eta, \tag{7}$$

and so a renormalization of ψ is needed: integrating over all space,

$$\int F(x)\,\mathrm{d}^3x=1. \tag{8}$$

3. The Ground-State Solution

While it is perhaps premature to devote much space to the details of specific states, it may be worth while to look at the ground state of a single electron bound to a nucleus of charge Z. We can omit the factor $\mathrm{e}^{i(E_0\tau-Et)/\hbar}$ (see (4)), and specify the wave function as follows:

$$\begin{aligned}&\xi_1=f(r),\\&\xi_2=0,\\&\eta_1=\epsilon\,f(r)\,\cos\theta,\\&\eta_2=\epsilon\,f(r)\,\sin\theta\,\mathrm{e}^{i\phi},\end{aligned} \tag{9}$$

$$\epsilon=\frac{\beta}{1+\gamma}=\frac{1-\gamma}{\beta}, \tag{10}$$

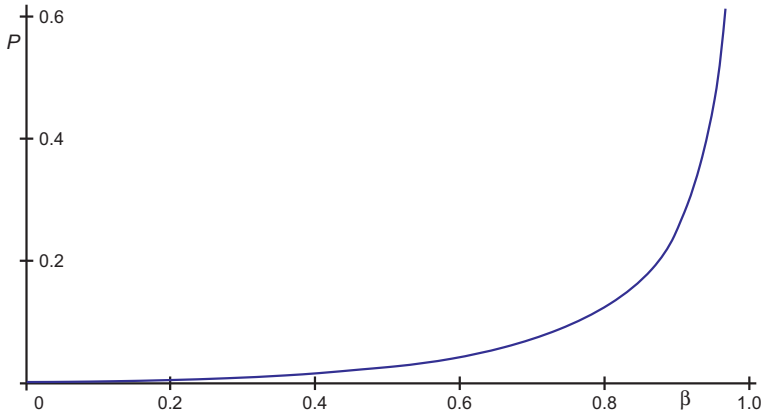

Figure 1. P, the space integral of the expected ground-state positron density, plotted against $\beta = \alpha Z$.

where $\beta = \alpha Z$ and $\gamma = \sqrt{1-\beta^2}$. Here we have the usual ground-state radial distribution function $f(r)$, of the form

$$f(r) = Kr^{\gamma-1}\mathrm{e}^{-\lambda r}, \tag{11}$$

where K is a normalization constant and $\lambda = \beta m_0 c/\hbar$. See, for example, [6], p.79 (where $c = \hbar = 1$), or for more details, [7], p.69. The normalization (8) implies that

$$4\pi(1-\epsilon^2)\int_0^\infty f^2(r)\,\mathrm{d}r = 1. \tag{12}$$

Using the relations above, we find that the expected positron density (along with the balancing part of the electron density) is

$$F_2 = f^2(r)\frac{\sqrt{1-\beta^2\sin^2\theta}-\gamma}{\gamma(1+\gamma)}. \tag{13}$$

For small β this gives $F_2 \approx \frac{1}{4}\beta^2 f^2(r)\cos^2\theta$, implying concentration around the polar axis. If we expand F_2 in powers of β, the second term is of order β^4, and so the lowest approximation is a good one until Z becomes quite large.

For the ground state, using F (as in (5)) instead of J^4 (as in (7)) makes no difference to the expected net charge density, because in this case $\xi^\dagger\xi$ and $\eta^\dagger\eta$ differ only by a constant factor. Nevertheless, the ground state predicted by the present 4-space model is different from that of conventional first-quantized Dirac theory, in that it already accommodates positrons. Having normalized F, we can use the integral of the expected positron density, i.e. $P(\beta) = \int F_2\,\mathrm{d}^3x$ (over all space), to indicate the cumulative departure from standard predictions of charge distribution. The result (using $\gamma = \sqrt{1-\beta^2}$, as above) is

$$P(\beta) = \frac{1}{4}\left[\frac{1}{\gamma} + \frac{\gamma}{2\beta}\ln\left(\frac{1+\beta}{1-\beta}\right) - 2\right]. \tag{14}$$

When β is small, $P(\beta) \approx \beta^2/12$. Although $P(\beta)$ diverges as $\beta \uparrow 1$, it remains relatively small until β reaches about 0.6, as the the graph (Fig. 1) illustrates. Hydrogenic uranium (U^{91+}) has $\beta \approx 0.67$, $P \approx 0.06$.

By increasing Z, we eventually reach a singularity when $\beta \uparrow 1$. Although one knows that it must be preceded by pair creation in an intense electric field, this phenomenon is normally predicted only after second quantization. In the present

4-space model, however, we already have an indication of the physics. To reach $P = 1$ we need $\beta \approx 0.9837$, corresponding to $Z \approx 135$. In the context of LENR, the point of these remarks, and of the graph of $P(\beta)$, is that the predicted effects of the 4-space formulation are small in relatively weak electric fields, but can become significant in strong fields. A further illustration is provided by the 4-space treatment of Klein's paradox [5].

4. Discussion

The model presented here is an attempt to describe, within a first-quantized framework, phenomena that are normally in the domain of second quantization. In this sense it is complementary to the efforts of Barut and others [8–12] to enlarge the scope of first-quantized theories.

The virtual-particle distributions described above are distinct from the more familiar vacuum polarization. Both can be thought of in terms of quasi-classical charge distributions, but when we consider the implications for tunnelling, this picture may not be adequate. If we accept it, then the virtual electrons and positrons of the 4-space Dirac theory (as outlined above) simply cancel each other out. In reality, however, wave functions do not describe continuous distributions of charge, but rather expected values for the occurrence of discrete charges. The associated potentials will therefore exhibit random fluctuations, implying that (with a low probability) large deviations from the average must occur. This suggests that under suitable conditions there could be a significant breakdown of the usual Coulomb repulsion between hydrogen nuclei. But because such a breakdown is mediated by individual electrons, the likelihood of its occurrence should decrease very rapidly as nuclear charge increases, effectively restricting the phenomenon to hydrogen.

Stochastic barriers have already been considered by Habib [13] and others. In the stochastic picture, low-probability extremes in barrier fluctuations are crucial, so that the fine detail of charge distributions takes on added significance. Concentration of virtual particles and antiparticles around an axis will make the extremes more likely, and thus provide a preferred route through a potential barrier. The foregoing description of the ground state shows that such effects can be much greater in the presence of strong electric fields. Even if the details outlined above do not apply in an actual LENR experiment, the breaking of symmetry (from spherical to axial in the ground state) can be expected to hold quite generally. In a lattice structure, especially, it may provide pathways along which low-energy hydrogen nuclei are more likely to have their mutual repulsion nullified by intervening electrons.

References

[1] J.R. Fanchi, *Found. Phys.* **23** (1993) 487.
[2] J.R. Fanchi, *Found. Phys.* **24** (1994) 543.
[3] A.B. Evans, *Found. Phys.* **20** (1990) 309.
[4] A.B. Evans, *Found. Phys.* **28** (1998) 291.
[5] A.B. Evans, *Found. Phys.* **21** (1991) 633.
[6] C. Itzykson, J.-B. Zuber, *Quantum Field Theory* (McGraw-Hill, New York, 1980).
[7] H.A. Bethe, E.E. Salpeter, *Quantum Mechanics of One and Two Electron Atoms* (Springer, Berlin, 1957).
[8] A.O. Barut, J. Kraus, *Found. Phys.* **13** (1983) 189.
[9] A.O. Barut, J.F. Van Heule, *Phys Rev.* A **32** (1985) 3187.
[10] A.O. Barut, J.P. Dowling, *Phys Rev.* A **36** (1987) 649.
[11] A.O. Barut, J.P. Dowling, *Phys Rev.* A **36** (1987) 2550.
[12] A.O. Barut, *Found. Phys.* **18** (1988) 95.
[13] S. Habib, *Proceedings, 4th Drexel Symposium on Quantum Nonintegrability* (1994). (arXiv:hep-th/9410181).

J. Condensed Matter Nucl. Sci. 2 (2009) 13–32

Research Article

Tracks of Ball Lightning in Apparatus?

E. H. Lewis*
Sciencejunk.org

Abstract

Researchers of electrical discharge and electrolysis experiments have been finding microscopic markings that are unusual and anomalous. It is possible that these markings are made by microscopic objects that are in the size range of 400–0.1 Åm. These objects may be a type of microscopic ball lightning. They may share the anomalous characteristics of natural ball lightning. They are also finding highly anomalous material activity and emissions. Pictures of the markings and anomalous effects that were taken by six groups of researchers are shown and interpreted in this article.

Keywords: Ball lightning, Plasmoids, Transmutation experiments, Microscopic ball lightning

1. Introduction

It is possible that microscopic ball lightning may leave microscopic markings and residual effects similar to those caused by natural ball lightning, tornadoes and experimentally produced plasmoids. Since 1992, Matsumoto, Dash et al., Shoulders, Lewis, Savvatimova, Urutskoev et al., Ivoilov and other groups have published pictures of microscopic ball lightning markings and effects, and the photographs show patterns of behavior that are identified and interpreted in this article. These effects can be classified as (1) the effect of ball lightning motion by moving or changing material: bore holes, scratches and trenches, and pits, (2) ball lightning radiation and emission effects, (3) residual markings such as trails and rings and residues, (4) areas of atomic motion such as heatless motion, sloshing, change of crystalline structure, phase transitions, the disappearance of atoms, crystals, dendrites and filaments, and (5) possible transmutation and isotopic residues.

It is possible that microscopic ball lightning exists. There is no reason, a priori, why this should not be so. First of all—the structure and composition of reported ball lighting in nature is not well understood. There seem to be various kinds. In prior articles, I have described how *macroscopic* ball lightning in nature vary greatly in size from centimeter to kilometer size (i.e. [1]). There is no reason why they might not also be micrometer size or smaller. The behavior of these objects, as evidenced by their tracks and effects, is like that of ball lightning, as explained in other articles [2–4], especially in how they bore and pass through materials like water, air, electrolysis cell walls, and paper (as Urutskoev

*E-mail: elewis@sciencejunk.org

reports [5]), and travel comparatively long distances in air before leaving interesting tracks in emulsions. Some ball lightning have been reported to pass through glass by making a hole in it, and some to pass though glass without making a hole in it. I have written about microscopic ball lightning now for 15 years [3, 4], and have been suggesting that people put detectors such as emulsions and CR-39 inside and outside their experiments. Urutskoev's report and some other evidence suggest that the "strange" objects are emitted even after the reactor parts are taken out and put in a Petri dish [5].

Also, there is some evidence of very unusual deposits left by BL. These deposits were possibly due to transmutation. Savvatimova has written that there is a correlation between number of markings found and the extent of transmutation in a given experiment. Matsumoto, Shoulders and Savvatimova have all written that the strange markings—the pits, tunnels, trenches and tracks—are locations of transmutation products.

Experimental researchers have produced interesting and beautiful pictures of microscopic ball lightning (MBL) and their effects that require explanation. People have experienced the anomalous behavior of natural BL and experimentally produced plasmoids, but a theory was lacking. One of the basic ideas presented in this article is that atoms may enter a state in which they behave anomalously. In 1991, Matsumoto published an article on elemental transmutation in which he showed microscopic voids with transmuted elements [6]. He published pictures of the anomalous microscopic markings left on electrodes and witness sheets (nuclear emulsions used for particle detection) during his electrolysis and discharge experiments. I hypothesized that microscopic BL were being formed at the site of the voids or that BL were causing the voids [3, 4]. After he received my correspondence, he started investigating microscopic ball lightning and published pictures of tracks of what I suspect are MBL. The many kinds of markings he and others have found are evidence the hypothesis is a valid one, since the markings show that the microscopic objects behave like natural ball lightning.

There is a state of existence of substance and space like that of natural BL. Objects in this state behave in ways that are anomalous to generally accepted theory. These objects may travel through materials, move anomalously such as in sharp angles without acceleration, move at low energies or low heat, transmute, combine to form bigger plasmoids, divide, emit plasmoids and beams, convert to energy, exhibit superconductivity and form interesting structures. These behaviors can be classified in the five categories of possible BL behavior explained in this article. Many of these behaviors are evidenced in the photographs shown here by the various researchers. These objects have been researched for decades, but only recently have the more anomalous BL-like behaviors been clear and a full theory is still lacking. These objects have been called by various names including EVs and charged clusters by Shoulders, EB filaments and plasmoids by Bostick and other researchers, ectons by Mesyats and other researchers, micro-ball lightning by Matsumoto, and microscopic ball lightning or tiny ball lightning by me.

The evidence is that these MBLs behave like the larger natural ones. Maybe BL smaller than a millimeter were not reported because they are difficult to see and people mistake the objects for something else. When I was a small kid, I may have seen BLs about 1 mm in size that I made by breaking a rock with a hammer, but I called them sparks. If I remember correctly, they changed colors, gave off a high-pitched sound, and one of them circled me and hit me on the wrist causing pain for a second, but left no mark. About 12 years ago, Matsumoto reported the microscopic markings left by natural MBL generated during the Matsumae earthquake in Hokkaido where he lives [7]. He was using special Acrylite plastic sheets called nuclear emulsions for artificial MBL experiments. One of the microscopic markings that he found on these sheets after the earthquake remind me of a hole left by a whirlwind type effect because there was a cone of material left intact inside a ring shaped pit and there was evidence of whirling behavior in the mark.

2. Five Classifications for Traces of BL

2.1. Class 1. The Effect of BL Motion by Removing Material: Bore Holes, Trenches and Scratches and Pits

BLs move though materials either by boring or without boring. One of the anomalous behaviors of natural BL is making holes in glass windows and in walls [8]. BL, tornadoes [1], and whirlwinds may move loose materials and pick up leaves, dirt, rocks and other objects. They sometimes leave trenches or grooves in the ground or on materials. The transported

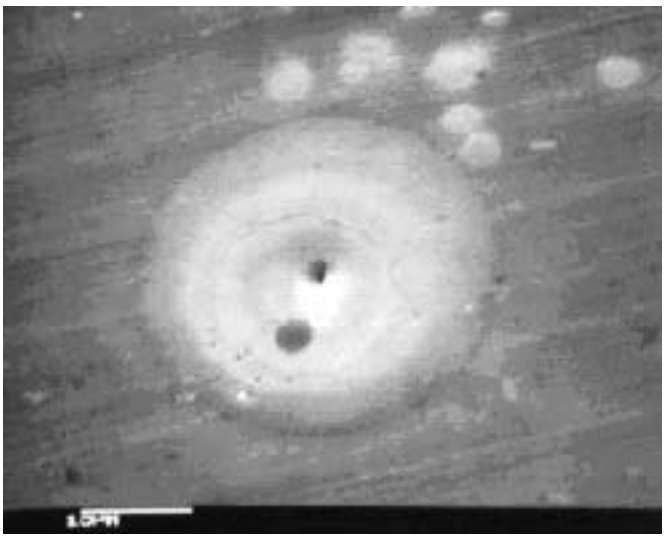

Figure 1. Entry pit of EV into aluminum sheet.

materials may revolve around these objects or may simply be moved by them. These behaviors are discussed in prior articles. Sometimes, BLs pass through glass windows without visible effect to the glass. The manner of passage of BL through material may depend on the properties of the material. For example, some windows were made with lead [9].

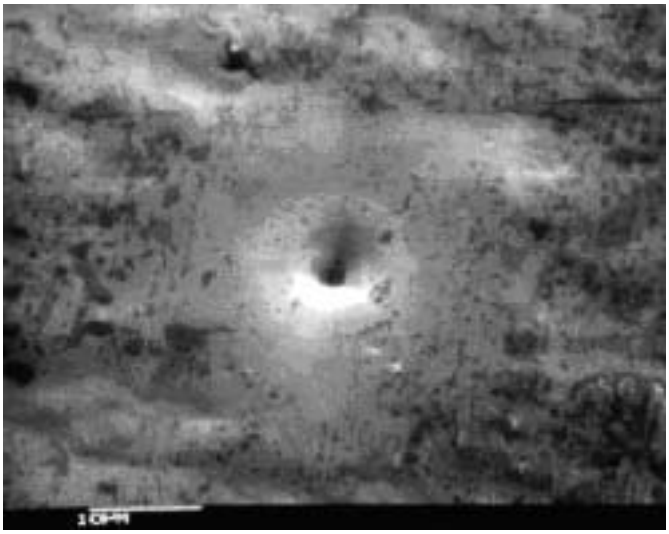

Figure 2. Opposite exit pit of EV from the sheet.

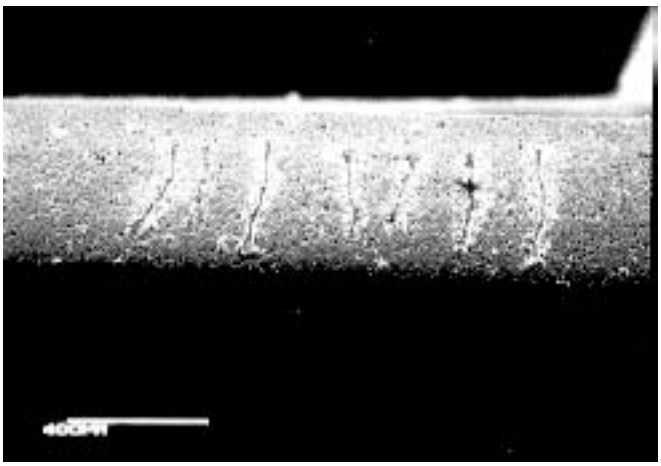

Figure 3. The scale is 400 μm.

Some of the microscopic objects Matsumoto produced experimentally may have passed though glass and plastic sheets without leaving an apparent hole before they left markings on his acrylite plastic nuclear emulsions.

Figures 1–3 show typical tunnel-like borings [10]. In Figs 1 and 2, the holes are in aluminum foil that is 6 μm thick, and are the entry and exit holes of a BL-like object. The pit in Fig. 1 is about 2 μm wide, and the one in Fig. 2 is about 3 μm wide. Perhaps the object grew as it passed through, which is a typical BL behavior. Figure 3 shows a cross section that shows EV boreholes through a 0.5 mm thick aluminum oxide plate. The aluminum oxide has a melting point of 2050^{o}C. This shows some of the power of these little objects to make holes.

Natural BL is often seen paired or in chains or rings of individual BLs. For example, someone reported a train of 25–30 blue globes the size of bowling balls roll rapidly down a mountain path during a thunderstorm [11]. This alignment is evident in Fig. 3. Roberto Giudici [12] took a picture of a four waterspouts that were in aligned in a straight row and look to be equally spaced on August 1999 near Albania in the Adriatic Sea. Prior articles will explain that I identify BL and tornadoes as types of the same general kind of plasmoid [1, 13]. BL often forms geometrical figures, and there are many reports of BL type objects moving in formation, splitting off or separating, and coming back

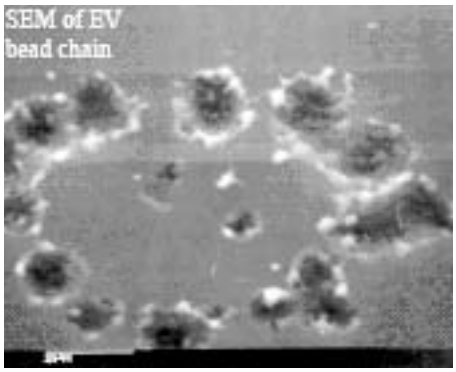

Figure 4. The scale is 25 μm.

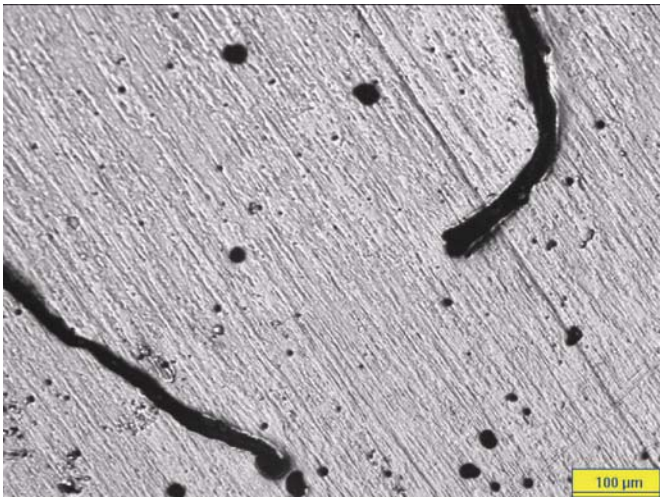

Figure 5. Scale here is 100 μm. Trenches in Palladium. About 50 μm Wide. Many Pits Also.

together again. BL acting in this way have been called UFOs. They exhibit spatial organization [14], and often mimic each other over long distances. Possibly this is why some tracks shown by researchers like Matsumoto and Ivoilov show mimicing motion of MBL. Perhaps atoms in a BL state would also exhibit such behavior, forming geometrical structures and showing organization and mimicing behavior. More about this is described later in the Class 4 section of this article.

Figure 4 [15] is a typical BL ring mark of pits arranged in a circle. Ball lightning often travel in ring formations,

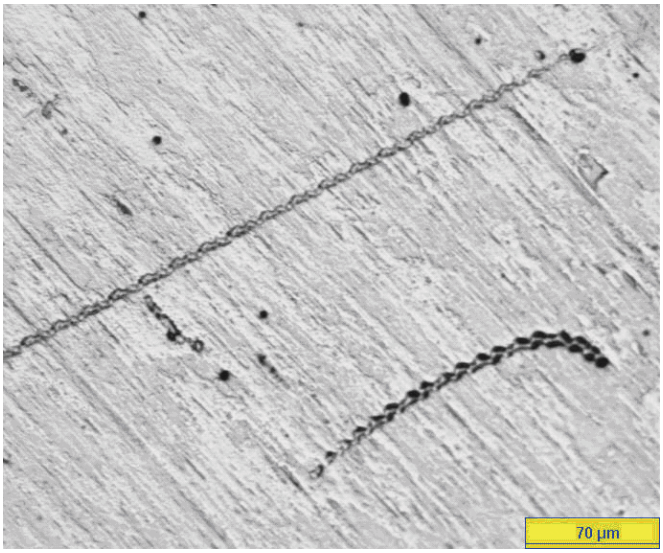

Figure 6. Scale here is 70 μm.

and when they contact material they may leave pits. Sometimes BL and tornadoes will leave a trench in the ground as they move. Here is one example. I have read several reports similar to this:

"A tornado or an accompanying fireball dug a trench in a hard-packed clay tennis court at Curepipe, Maritius, in the Indian Ocean, on May 24, 1948: A trench running in a north-south direction, 60 feet long and 1–2.5 feet wide, was cut in the bare surface of the court to a depth varying from 1 to 4 in. The material lifted from the trench was all thrown to the west to a distance of 50 feet; pieces weighing about one pound were thrown as far as 30 feet. The surface material was slightly blackened as if by heating, and a crackling that of a sugar-cane fire was heard for 2 or 3 min. One claims to have seen a ball of fire about two feet in diameter which crossed from a football pitch to the tennis court through a wire-netting fence without leaving any evidence of it passage [16]".

Maybe the trench-like markings in the next several pictures were caused by a similar effect. People may find ball lightning deposits like that described in the quotation just above. In Fig. 5, Savvatimova found these trench-like marks and pits in the surface of palladium used in a glow-discharge experiment [17] that are due to the movement of BL over the surface. Some tornadoes and BL were reported to hop up and down making holes, and as was explained previously [18] some of the markings shown by Matsumoto show the same effect of hopping. See for example, the picture by Matsumoto in this article.

Figure 6 was also taken by Savvatimova and shows two BL trail-like markings in palladium [17]. The top linear mark may show that a BL entered the pit or made the pit, since the track ends at the pit. Notice the short, thin, shallow trench mark below the long one that crosses the picture. Tracks like that one remind me of marks in the 1993 article by Silver et al. [19] and in components of one of Miley's experiments [20,21]. There was a pit in a titanium electrode in that experiment with marks that appeared sort of like rings and shallow grooves in the picture I took (see Fig. 4 of ref. [18]; the picture did not print as clear as the original). Many of the pictures taken during this decade by Urutskoev and Savvatimova show a pattern of repeating patterns in a line, like these long ones and like others discussed below. In this article and in other articles, I speculate about the cause for the various markings. But the idea of revolving MBL as an explanation for spiral marks such as those in Figs. 11 and 14 in this article might be a good idea.

Figure 7 taken by Savvatimova may show that a BL made pits in palladium [17] as it traveled in a fairly straight line. The pits may be connected by a shallow and narrow trench mark. There are other such marks. It seems less likely to me that a string of MBL left the string of pits. Brush discharge markings connected plasmoid pits and rings in a picture shown by Nardi et al. [22] that are similar to some of the others shown in this article, but the thin lines between the pits in the above figure do not look like brush discharges.

Figures 8 and 9 show ring marks on the microspheres from an experiment by Miley et al. [20] taken by me [21]. As explained previously [18], this cell registered the highest recorded energy output of various microsphere runs. Compare these three rings to the one by Shoulders in Fig. 4. Figure 8 shows two rings of pits in the metal coating of the microsphere [20, 21]. Also Fig. 9 shows a faint white ring in the plastic substrate of a microsphere [20, 21]. This copy of the photograph is not as clear as the original.

Figure 10 was an optical photograph taken by Shoulders [15] of a revolving pair of EVs loosening up. In nature, two or more BLs and tornadoes often revolve. Shoulders used a special form of particle sensitive camera. The photograph is included to compare it with the marking on the electrode shown in Fig. 11 and the trace on X-ray film shown in Fig. 14a. The evidence is that the plasmoids he has researched are individual objects that form larger structures such as pairs, rings and strings.

Figure 11 was taken by Savvatimova and shows the mark of a BL or maybe a pair of them [17] which left a dark mark on the surface of the palladium used by Savvatimova. I am speculating that the mark was made by a revolving MBL or a couple of MBLs that were revolving.

Could the trenches, tunnels, ring marks, pits and other markings be made by a beam of some type and not by individual objects? People have reported that beams are associated with low energy transmutation, but the evidence is that the markings discussed in these pictures were not made by beams, but by individual objects. Ken Shoulders

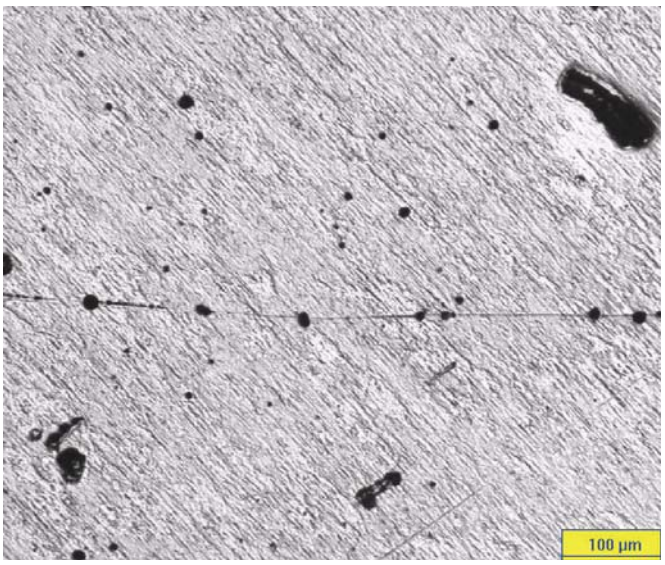

Figure 7. Scale is 100 μm. Maybe an MBL hopped or skimmed along and made this line of pits. Perhaps this was caused by a chain of MBLs.

told me that EB-filaments studied by Bostick, Nardi, and other researchers were found later to be individual objects traveling very fast when a very fast camera was used [23]. K. Shoulders has recently written that Winston Bostick came to recognize that the plasmoids he studied, also called EB-filaments, were composed of the EVs. For example, Shoulders wrote: "…Winston did his work, he did not know that EVs were the main component of his plasmoids. Years later, when I employed him as a consultant on EV technology, he came to see the effect and love it. [24]".

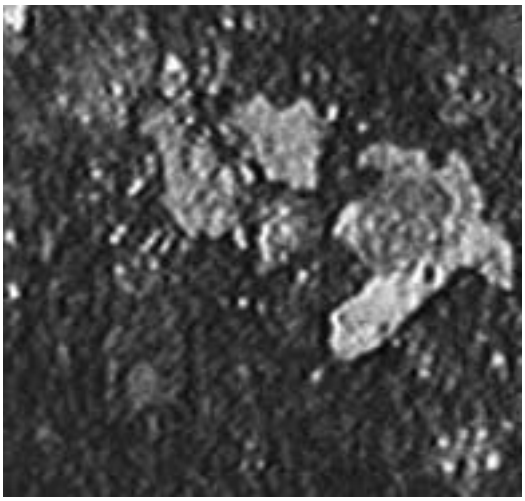

Figure 8. Two rings of pits in thin film of Ni on a plastic microsphere. The microsphere was in Miley's Ni on plastic run No. 8 experiment.

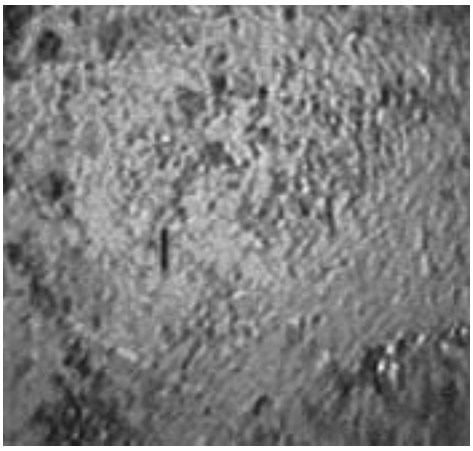

Figure 9. Faint ring in plastic microsphere. There are light colored pits in a ring just above the black line I drew.

Maybe the pictures here show two ways that MBL leave holes. One way is by boring, and the other is by drilling without passing through, like a tornado. As an example of the second way a BL makes holes, Egon Bach reported that two large BL-like objects drilled holes in the ground in the Soviet Union [25]. A slightly flattened glowing ball about 400 m in diameter hung for an hour low over the ground over the same spot—only 1 km from seven observers. Afterward, they found a huge hole that they thought the object had probably dug. No trace of the excavated material could be found. Another group of seven men saw a similar, smaller red object about 3 km away from the first. Professor Zolotov was asked to study the holes. One of the strange holes was three to 4 feet wide but 30–40 feet deep. It widened to 8 feet in diameter at the bottom. The walls were covered with a layer of carbon dust about 0.2 mm thick. The carbon fiber had a radiation three times above normal [25].

Figure 10. Optical picture of revolving EVs. Taken with a special camera. From Shoulder's article. See how similar this looks to Figs. 11 and 14.

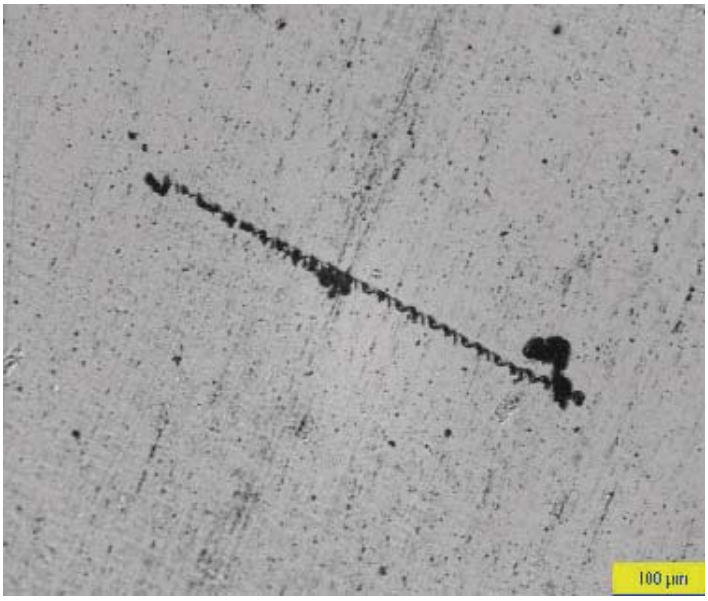

Figure 11. Marking in Palladium by Savvatimova.

The carbon dust is an example of residues left by BL as discussed in the section for Classification 3. Carbon residues have been reported by Matsumoto and Savvatimova and some other CF researchers.

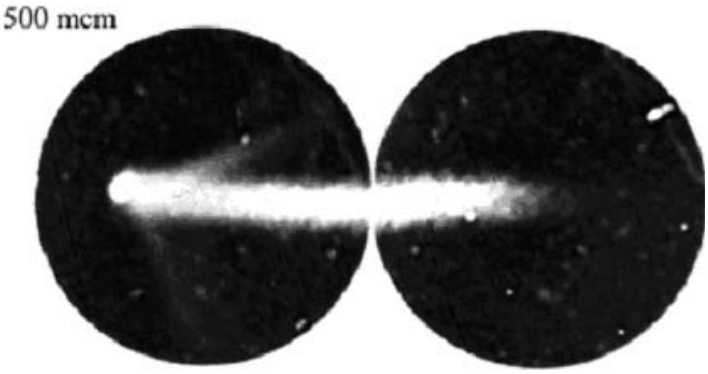

Figure 12. Comet-like marking with rays. Photograph by Urutskoev et al.

Figure 13. Ring marks + trail marks on nuclear emulsion.

2.2. Class 2. Ball Lightning Radiation and Emission Effects

These objects emit particles, beams, sound, light, electrical discharges, and plasmoids of various kinds. Most BL photographs are not actually a photograph of the object itself, but of the streak of light caught by the camera as it

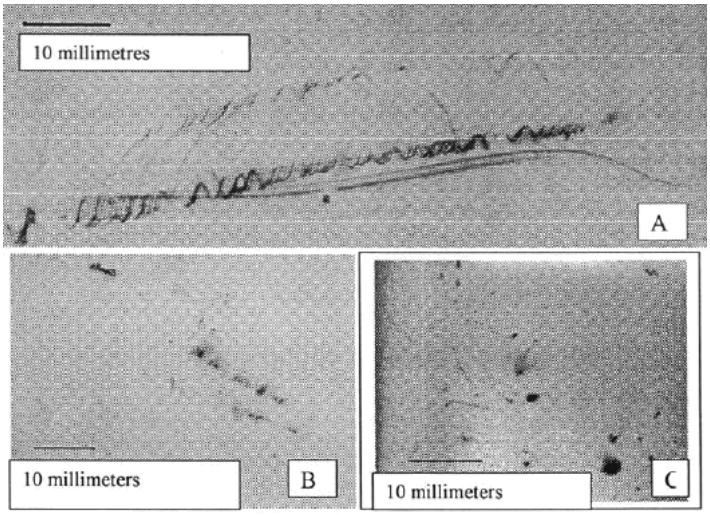

Figure 14. Markings on X-ray films set outside (A,B) and inside (C) vacuum chamber. Deuterium irradiation in glow discharge. The mark in A may record a spiral motion of an MBL or a revolution of two MBLs. The ones in B look like the ones Matsumoto called interference patterns. The ones in C look like ones Matsumoto photographed as well.

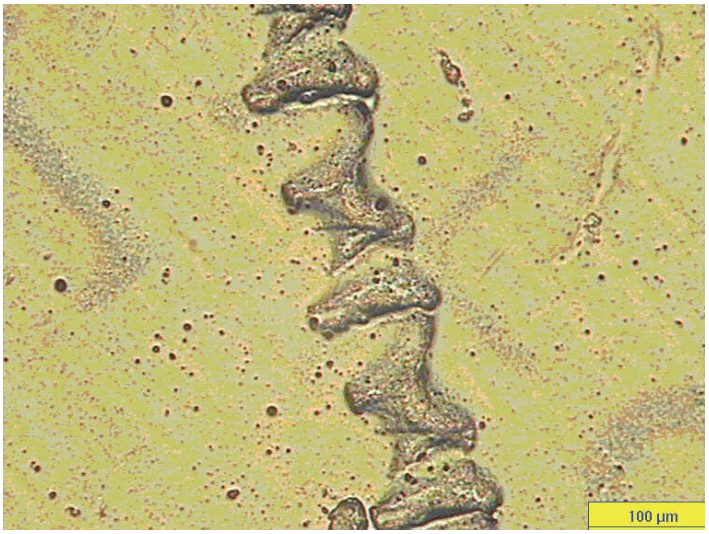

Figure 15. Residual trail mark on emulsion. It is about 100 μm wide. Urutskoev and Savvatimova have called patterns like these "tire-track" markings. At lower magnifications, they look like dark lines The scale is about 100 μm.

moved, like the optical photograph by Shoulders shown in this article. According to Feugeas, the EB-filaments that he studied with Nardi and Bostick traveled at a speed of .76 of the speed of light [26]. People photographing fast moving plasmoids may have thought that they photographed a beam or a current. I suspect that the dark path in Fig. 11 is a streak of the light emitted from the plasmoid moving over the surface.

These objects emit neutrons and other particles. Nardi et al. [22] reported that their plasma focus discharge device containing deuterium oxide produced neutrons. Lightning is known to produce neutrons [27], and Dijkhuis and Pijpelink [28] reported neutrons during their experimental study. One trace shown by Matsumoto in his articles which he called a "superstar trace" (Fig. 8 in [29]) showed some types of particles or small plasmoid emission from a larger BL-like object that moved on the plastic sheet. A similar track without marks of emissions is shown in Fig. 3e of Ref. [30]. BL and MBL discharge electricity. Some of Matsumoto's and Urutskoev's markings show the emission of beams or rays of some type. For example, Fig. 2b of Matsumoto's article [30] shows a mark like a discharge from the object. The emission of beams, rays or sparks of some type are commonly reported about BL [11].

Figure 12 taken by Urutskoev shows emission from the MBL that made the trace registered on a nuclear photoemulsion [31]. I am assuming that the long streak is a MBL track made by the light emitted from MBL. One can see that there was emission of rays or flares from the MBL. He wrote: "Six such 'comets' were detected inside the area 4 cm^2. Their sizes varied from 300 to 1300 mcm" [31]. They look like markings Matsumoto called traces of "white holes" in his article in *Fusion Technology* [30]. Urutskoev wrote that these markings evidence very high energy. However, they also traveled a long distance through air, and through black paper and the container of this experiment. Ball lightning acts like this.

2.3. Class 3. Residual Markings Such as Trails and Rings and Residues

Unlike a trench or pit marking due to the removal of material, this type of marking may be the deposition of a residue of some type or a chemical change that colors materials.

Figure 16. A trail marking on nuclear emulsion. From deuterium glow discharge experiment with W–W cathodes. The scale is 100 μm.

Figure 13 [32] is like another Matsumoto has shown on acrylite plastic nuclear emulsions showing both ring and trail marks as if MBL translated and hopped on a nuclear emulsion in a tornado-like manner. In this picture, one MBL may have been responsible for all the marks [1, 13].

Figure 14 shows markings on X-ray film outside (A, B) and inside the vacuum chamber after deuteron irradiation in glow discharge [33]. Figure 14a may show the trace of a MBL moving in a spiral motion or of two MBLs revolving. The blots in Fig. 14c look like the round dark spots on emulsions shown by Matsumoto [30] and may be like the round spots shown by Urutskoev in Fig. 16c of his article [31]. The spiral in Fig. 14a opens from right to left, and looks similar to Shoulder's photograph in Fig. 10.

Figure 15 is by Savvatimova of a marking on nuclear emulsion placed around a glow discharge chamber [17]. She found many such markings on emulsion set both inside and outside the chamber. It is about 100 μm wide. The fainter light colored marking to the right which is about 15 μm wide, seems more similar to the clear long track markings on nuclear emulsions which Matsumoto called "loop-like [29]" traces (group 6 of Ref. [29]), which I thought were due to either some type of sloshing or shallow indentation of MBLs moving in contact with the emulsions. Urutskoev [31], Ivoilov [34], and Savvatimova have published these kinds of patterned tracks. This one looks like deposits or segmented areas of a change of the chemical composition of the emulsions. One MBL may leave different kinds of markings as it travels along. For example, one may make a continual line track and then make this kind of track. See for example, Fig. 18.

Figure 16 is a marking on nuclear emulsion [17]. This may be a record of the radiation that the MBL was emitting. It looks like a marking shown by Matsumoto in Fig. 3c,d of Ref. [30] that seems to show two objects that mimicked each other moving in opposite directions on an emulsion. Figure 3c has a light colored boundary and Fig. 3d has a dark boundary. These two figures are simply different focusing of the microscope on the same track. But the track in Fig. 3d of that article by Matsumoto looks much like this Fig. 16. I am wondering if this may be the reason for the thick, dark border in Fig. 16.

One of the anomalous behaviors reported about some BL and UFO objects is sharp angled turns without any

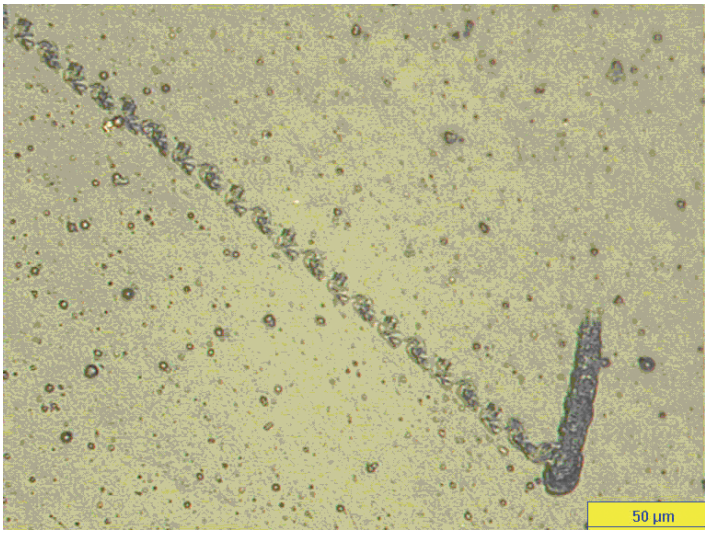

Figure 17. Sharp angle turn track on X-ray film.

deceleration. This unusual movement probably attracts the attention of observers, and is why people called them UFOs. Planes do not move in this way. Another anomalous behavior of MBL is that groups of them may mimic each other's motions, and they may divide, move in patterns, and come back together again. Sometimes they are

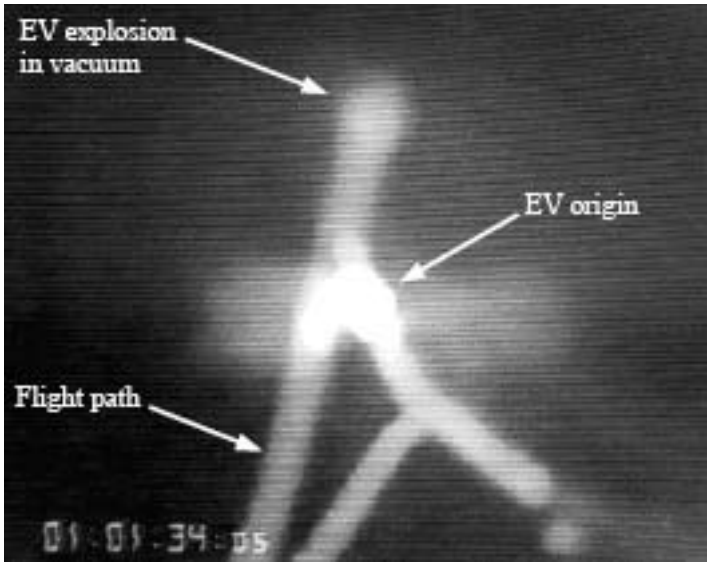

Figure 18. EV picture showing sharp angle turn. The sharp turns are on the right side of the picture.

reported to repeat a pattern of motion several times. Ivoilov has photographed tracks showing mimicing, sharp angled movement of microscopic objects [34]. The tracks may evidence angular motion without acceleration or curvature. This is characteristic of MBL (see Figs. 17 and 18).

In Fig. 17, a sharp angle of turn of MBL may be recorded in emulsion [17]. The track appears to be a chemical change or a deposit on the emulsion. From the looks of it, a MBL moved downwards leaving the thick stroke, backtracked slightly and then made the segmented track. The last position of the object on the thicker streak was at the intersection with the segmented track. I am speculating that some type of revolving or rotating motion may be involved. The object might have been round because a round mark is evident at the point of intersection.

Figure 18 is a photograph showing a sharp angle turn by Shoulders [15]. As he explained, it is evident that there was no acceleration at the turns because the path shows the same brightness throughout. It is interesting that this photograph may also show that the object backtracked, as an MBL may have done on the emulsion shown in Fig. 17.

2.4. Class 4. Areas of Atomic Motion such as Heatless Motion, Sloshing, Change of Crystalline Structure, Phase Transitions, the Disappearance of Atoms, Crystals, Dendrites and Filaments

Two ways atoms may move anomalously are as the result of BL contact or influence and due to stresses. Atoms may move and reorganize in the presence of BL leaving crystals or changing the crystalline structure or phase structure of material. Stressing materials or substances may cause the formation of BL or the emission of plasmoids of various kinds, or cause atoms be in the anomalous state [2, 4, 18] to exhibit qualities such as superconductivity [4, 35], anomalous motion at temperatures below their melting point [4], and change crystalline structure or phase transition [4, 35]. For example, Lipson's early experiments on superconductivity and cold fusion effects showed that when a sample of HTSC $YBaCu_3O_{7-x}$ was heated [4, 36], starting from 77^o, there was definite neutron emission accompanying the loss of superconductivity and the phase transition to a non-superconducting state. Zhukov and Egorov have written that researchers who study the behavior of electrodes during electrical discharge know that "intense electric fields acting on the emitting surface cause a thin layer with liquid-like properties to form at temperatures below the melting point" [37]. The rings in the layer they photographed reminded me of sunspots.

Figure 19 was taken by Dash and shows pictures of a Ti cathode before and after electrolysis and of a magnified scratch mark showing some sloshing on the side [38]. As another example of anomalous "melting" behavior, atomic motion without heat, Benjamin Franklin researched the phenomenon of lightning striking metals inside insulating material such as clothing and seemingly merging together as if by melting without scorching the material [4, 18]. He called this strange effect "cold fusion." I think that this anomalous state of atoms exemplified by behavior like this is part of the key to understanding cold fusion. CF phenomena, and I suspect superconductivity [4] and many other anomalous behaviors, occur when atoms are in this state. Researchers such as Dash have noted the anomalous appearance of crystals, areas of apparent melting, and metal deformation during electrolysis. Based on the observations of researchers, it is known that even after an experiment is finished, there is continued transmutation, change of metal morphology, growth of filaments and strange structures [38], radiation, and emission of microscopic objects that act like ball lightning [5]. This is evidence of a previously unknown state of substance [4, 18].

Figures 20 and 21 show filaments that grew on electrodes used by Dash [38]. According to Dash [39], Mizuno found similar growths. In Fig. 21, if you look closely, you will see that the particular fiber they analyzed looked different over time. The fibers in Fig. 21 are particularly anomalous because they grew and changed after the experiment was long over.

As explained previously, it is hypothesized that there exists a state of substance which exhibits anomalous properties [2, 4, 18, 35]. Atoms in this state may tend to organize in geometric patterns. As shown by the mimicing tracks in Iviolov's ICCF11 presentation [34], Fig. 3c,d of Ref. [30] by Matsumoto, and Shoulders' research, plasmoids have a tendency to mimic each other even over relatively long distances when they are in a group. BL mimic each other in

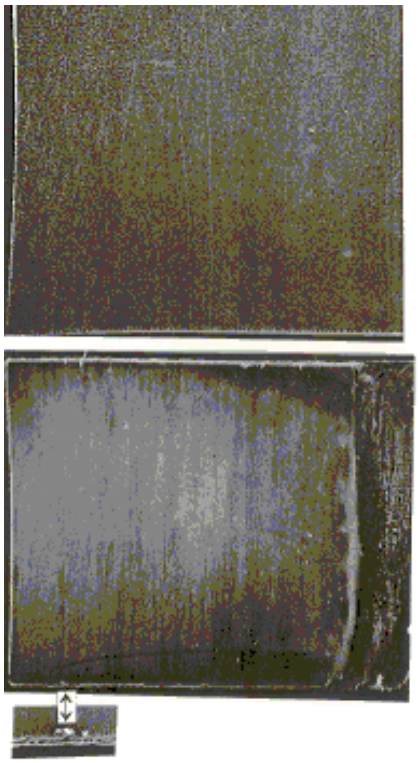

Figure 19. Trench on Ti cathode with sloshing on the sides.

this way in a group. This is how they form groups.

2.5. Class 5. Possible Transmutation and Isotopic Residues

The various researchers report a relationship between the emission of anomalous microscopic objects and transmutation and isotopic changes. These microscopic objects may possibly be microscopic ball lightning. Matsumoto's transmutation experiments show this correlation, and Savvatimova wrote, "There are more tracks for experiments with increasing new elements on the cathode surface [33]." In Ref. [10], Shoulders wrote that the only places on their deuterium loaded Pd that exhibited elemental changes were those places struck by the EVs [10]. There have been reports of residues left by UFOs that were highly unusual in that there were radioactive isotopes and rare and very heavy elements and other unusual materials. I speculate that these were simply large BLs. More evidence of this possible connection between MBL and transmutation is that the microsphere cell Run No. 8 in Miley's lab has many markings [18, 21].

3. Conclusion

It is possible that microscopic sized ball lightning exists, because there is not reason, a priori, that they should not. Anecdotal reports of things that may be called ball lightning in nature describe effects and behavior that are highly unusual, but similar to that of cold fusion. These reported behaviors including luminosity, explosions, emissions of

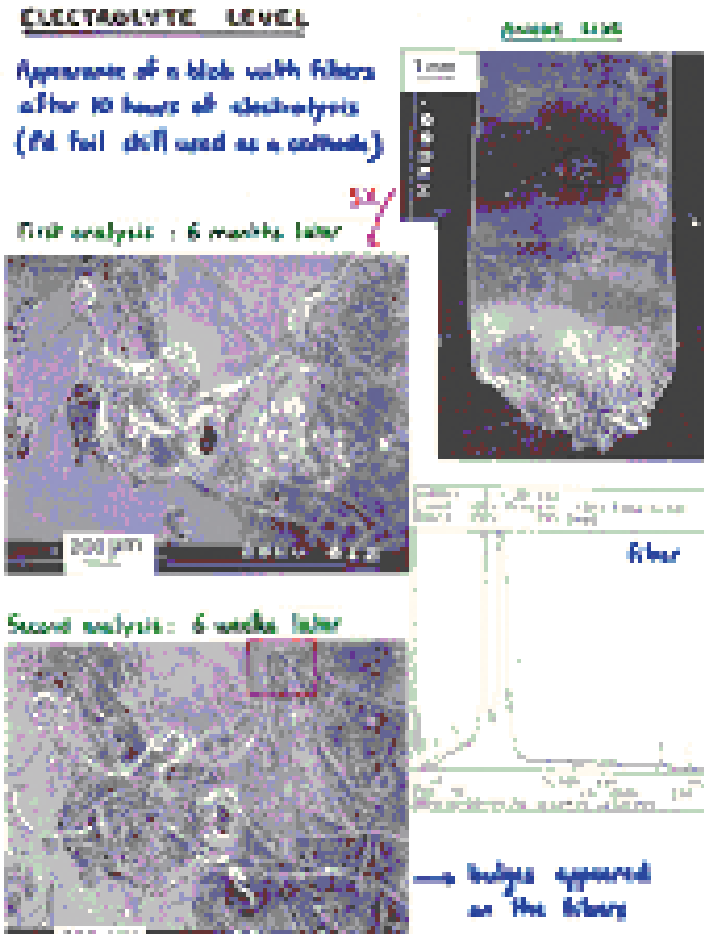

Figure 20. Fibers that grew during electrolysis.

beams and sparks, high radiation, leaving strange residues, leaving heavy or rare elements, passing through glass without leaving holes, passing through materials by boring holes, leaving pits and trenches, moving material, moving in geometrical patterns, dividing and coming together again, and forming groups of rings, lines, or equilateral figures like triangles or parallelograms [14] are all exhibited by the microscopic objects emitted from transmutation experiments. This is evidence for the possible existence of ball lighting that are extremely small and of their possible role in transmutation experiments. Ivoilov showed tracks that evidence complicated mimicing motion of these objects over long distances and of sharp angled turns without acceleration. Perhaps this kind of motion is analogous to known natural BL behavior. Shoulders showed that experimental plasmoids evidence sharp turns without acceleration. Similar tracks have now been observed by about seven groups of researchers.

Based on the report by Pryakhin et al. [40] and other reasons, I would like to warn people investigating transmutation and MBLs that the microscopic emissions may be hazardous. They ran a preliminary study on mice next to Urutskoev's

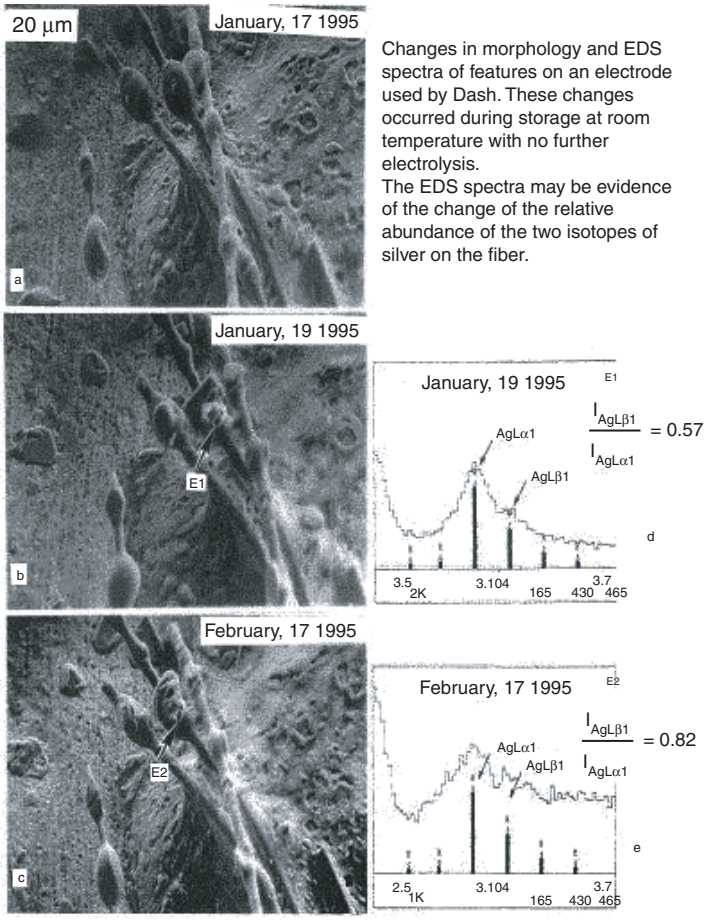

Changes in morphology and EDS spectra of features on an electrode used by Dash. These changes occurred during storage at room temperature with no further electrolysis.
The EDS spectra may be evidence of the change of the relative abundance of the two isotopes of silver on the fiber.

Figure 21. Fibers that grew on the electrode after an electrolysis experiment during 1 month with EDS charts.

experiments producing the "strange radiation" as they call it, and found that the mice were affected after only a few days. Ball lightnings have killed and injured people.

It is hypothesized that atoms enter an anomalous state in contact with MBL [4, 18] or when subjected to stresses. Atoms may remain in this state long after the cause is gone. It is this state that may explain the reports of anomalous behavior of atoms after the end of experiments, and during experiments. This article was written to summarize some evidence for microscopic BL, to explain evidence relating MBL to plasmoids produced experimentally by researchers like Shoulders and Bostick, to summarize the recent (post 2000) experimental evidence and relate the work to earlier results, and to attempt to explain the kinds of MBL effects people have been discovering experimentally.

Acknowledgment

I would like to thank Savvatimova, Shoulders, Matsumoto, Dash, and Urutskoev for permission to use the pictures. Two photographs were taken by E. Lewis of various components of Ni-Plastic Run No. 8 in the laboratory of Professor Miley at the University of Illinois in 1996. His cooperation in allowing this work is gratefully acknowledged. This is a very modified version of a paper that was published previously: Lewis, Traces of ball lightnings in apparatus, in: *Proceedings Second International Symposium on Unconventional Plasmas, ISUP-06, Eindhoven, The Netherland, August 14–16, 2006.* Editors D.K. Callebaut, G. C. Dijkhuis and H. Kikuchi [2].

References

[1] E. Lewis, Tornadoes and ball lightning, *Infinite Energy* **5** (2000) 65.
[2] E. Lewis, Traces of ball lightnings in apparatus, in: *Proceedings Second International Symposium on Unconventional Plasmas, ISUP-06,* Eindhoven, The Netherland, August 14–16, 2006.
[3] E. Lewis, A proposal for the performance of four kinds of experiments to test my own hypotheses and a statement of a deduction about phenomena, manuscript article, dated October 19, 1992.
[4] E. Lewis, A description of phenomena according to my theory and experiments to test it, manuscript article, Dec. 1992.
[5] L.I. Urutskoev, V.I. Liksonov, V.G. Tsinoev, Observation of transformation of chemical elements during electric discharge, manuscript, 2001, available at http://arxiv.org/abs/physics/0101089.
[6] T. Matsumoto, K. Kurokawa, Observation of heavy elements produced during explosive cold fusion, *Fusion Technol.* **20** (1991) 323–329.
[7] T. Matsumoto, Extraordinary traces on nuclear emulsions obtained during the Matsumae Earthquakes in 1996, in: *Proceedings of the Sixth International Conference on Cold Fusion, Progress in New Hydrogen Energy*, Lake Toya, Hokkaido, Japan, October 13–18, 1996.
[8] G. Egely, Physical problems and physical properties of ball lightning, in: *Proceedings of the First International Symposium on Ball Lightning (Fire Ball)—The Science of Ball Lightning (Fire Ball)* Tokyo, Japan, July 4–6, 1988, World Scientific, Singapore.
[9] K. Shoulders, personal e-mail.
[10] K. Shoulders, S. Shoulders, Charged clusters in action, manuscript article, 1999.

[11] S. Singer, *The Nature of Ball Lightning* (Plenum, New York, 1971).
[12] R. Giudici, available at <http://www.ernmphotography.com/Pages/Ball_Lightning/OtherBLPages/fbparks/BL_Triple_Waterspout.html>.
[13] E. Lewis, Tornadoes, ball lightning, and tiny plasmoids in devices, *Frontier Perspectives* **6**(2) (1997) 79.
[14] E. Lewis, Reply to "Comments on 'Transmutation in a gold-light water electrolysis system,"' *Fusion Technol.* **37** (2000) 266.
[15] K. Shoulders, Permittivity transitions, manuscript article, 2000.
[16] *Weather* **4** (1949) 156–157.
[17] B. Rodionov, I. Savvatimova, Unusual structures on the material surfaces irradiated by low energy ions and in other various processes, in: *Proceedings of the 12th International Conference on Condensed Matter Nuclear Science* Yokohama, Japan, November 27–December 2, 2005.
[18] E. Lewis, The ball lightning state in cold fusion, in: *Proceedings of the Tenth International Conference on Cold Fusion* Boston, Massachusetts, August 24–29, 2003 (World Scientific, Singapore).
[19] D. Silver, J. Dash, P. Keefe, Surface topography of a palladium cathode after electrolysis in heavy water, *Fusion Technol.* **24** (1993) 423–430.
[20] G. H. Miley et al., Quantitative observation of transmutation products occurring in thin-film coated microspheres during electrolysis, in: *Proceedings of the Sixth International Conference on Cold Fusion,* Hokkaido, Japan, October 14–17, 1996**.**
[21] E. Lewis, Photographs of some components of an electrolysis cell, web article, 1997.
[22] V. Nardi, W. Bostick, J. Feugeas, W. Prior, Internal structure of electron-beam filaments, *Phys. Rev. A* **22** (1980) 2211.
[23] K. Shoulders, Personal conversation, Sept. 1996.
[24] K. Shoulders, Electron condensors, manuscript article, dated Sept. 14, 2004.
[25] E. Bach, "*UFO'S" From the Volcanoes* (Hermitage Publishers, Tennafly, NJ, 1993).
[26] J. Feugeas, Comments on "Evidence of micrometre-sized plasmoid emission during electrolysis cold fusion," *Fusion Sci. Technol.* **40** (2001) 109.
[27] G. Shah, H. Razdan, C. Bhat, Q. Ali, Neutron generation in lightning bolts, *Nature* **313** (1985) 773.
[28] G. Dijkhuis, J. Pijpelink, Performance of a high-voltage test facility designed for investigation of ball lightning, in: *Proceedings of the First International Symposium on Ball Lightning (Fire Ball)—The Science of Ball Lightning (Fire Ball)* Tokyo, Japan, July 4–6, 1988 (World Scientific, Singapore).
[29] T. Matsumoto, Observation of gravity decays of multiple-neutron nuclei during cold fusion, *Fusion Technol.* **22** (1992) 165.
[30] T. Matsumoto, Searching for tiny black holes during cold fusion, *Fusion Technol.* **22** (1992) 281.
[31] L.I. Urutskoev, V.I. Liksonov, V.G. Tsinoev, Observation of transformation of chemical elements during electric discharge, *Annales Fondation Louis de Broglie* **27** (2002) 701.
[32] T. Matsumoto, Observation of tiny ball lightning during electrical discharge in water, manuscript article, 1994.
[33] I. Savvatimova, Reproducibility of experiments in glow discharge and processes accompanying deuterium ions bombardment, in: *Proceedings of the Eighth International Conference on Cold Fusion,* Lerici, Italy, May 21–26, 2000.
[34] N. G. Ivoilov, Low energy generation of the "strange" radiation, Powerpoint demonstration for the ICCF11, Marseille, France, October 31–November 5, 2004, available at <http://www.iscmns.org/iccf11/ppt/IvoilovNStrange.ppt>.
[35] E. Lewis, Considerations about plasmoid phenomena and superconductivity phenomena, manuscript article (1996), available at <www.sciencejunk.org>.
[36] A. Lipson, D. Sakov, Yu. Toporov, V. Gromov, B. Deryagin, Possible cold nuclear fusion in the deuterated ceramic $YBa_2Cu_3O_{7-x}$ in the superconducting state, *Soviet Physics Doklady* **36** (1991) 49.
[37] V. M. Zhukov, N. V. Egorov, Study of the appearing rings in the emission image of a field emission cathode prior to explosion, *Soviet Phys. Tech. Phys.* **36** (1991) 353.

[38] J. Dash et al., Research at Portland State University on the interaction of metals with hydrogen isotopes, Powerpoint demonstration.
[39] J. Dash, personal e-mail, 2006.
[40] E. A. Pryakhin, L. I. Urutskoev, G. A. Tryapitsina, A. V. Akleyev, Assessment of biological effects of "strange" radiation, Powerpoint demonstration for the ICCF11, Marseille, France, October 31–November 5, 2004, available at <http://www.iscmns.org/iccf11/ppt/PriakhinEABological.ppt>.

J. Condensed Matter Nucl. Sci. 2 (2009) 33–44

Research Article

Dynamic Mechanism of TSC Condensation Motion

Akito Takahashi *

Technova Inc., 13th Floor, The Imperial Hotel Tower, 1-1, Uchisaiwai-cho 1-chome, Chiyoda-ku, Tokyo 100-0011, Japan

Abstract

This paper discusses and explains the time-dependent quantum-mechanical behavior of electron-clouds in 4D/TSC (tetrahedral symmetric condensate) condensation motion by the Langevin equation, in comparison with steady ground state electron orbits and their de Broglie wave lengths for the D-atom and D_2 molecule. An electron orbit in a "d–e–d–e" quasi-molecular system of a face of 4D/TSC under time-dependent condensation makes a spiral track, finally reaching the center-of-mass point of the TSC, with a tail of time-varying effective wave length. The role and merit of the heavy mass electronic quasi-particle expansion theory (HMEQPET) method for approximating time-dependent TSC trapping potential and relating it to the estimation of time-dependent Coulomb barrier penetration probabilities of a 4D cluster is explained.

Keywords: Tetrahedral symmetric condensate, 4D cluster, condensation motion, Langevin equation, Time-dependent trapping potential, Barrier penetration, Fusion rate

1. Introduction

The formation of 4D/TSC (tetrahedral symmetric condensate) at or around a T-site of a regular PdD lattice under D-phonon excitation; or on the topological (fractal) nano-scale surface of PdDx; and/or along the interface of metal–oxide–metal nano-composite, has been proposed as the seed of deuteron-cluster fusion, which produces heat with helium-4 as 4D fusion ash [1]. The dynamic motion of TSC condensation was quantitatively studied by the quantum-mechanical stochastic differential equation (Langevin equation) for many-body cluster systems of deuterons and electrons under Platonic symmetry [2–6].

By the ensemble averaging of the Langevin equation with the weight of quantum mechanical wave-functions for electrons and deuterons, we could further derive a time-dependent one-dimensional Langevin equation for expectation value $\langle R_{dd} \rangle$, which is nonlinear, but could be solved by the Verlet's time-step method [2,3]. We showed in our previous work [4] that only 4D(or H)/TSC, among D_2, D_2^+, D_3^+, 4D/TSC and $6D^{2-}$/OSC clusters, can condense ultimately to form a very small charge-neutral entity, with a radius of about 10–20 fm. At the final stage of 4D/TSC condensation in about 2×10^{-20} s, 4D fusion with two ^{4}He products takes place with almost 100% probability, according to our heavy

*E-mail: takahashi@technova.co.jp or akito@sutv.zaq.ne.jp

mass electronic quasi-particle expansion theory (HMEQPET) calculation [3,4] for barrier factors and the fusion rate formula by Fermi's first golden rule.

This paper presents further discussions and explanations of the time-dependent quantum-mechanical behavior of electron clouds in 4D/TSC condensation motion, in comparison with steady ground state electron orbits and their de Broglie wave lengths for the D-atom and D_2 molecule. An electron orbit in a "d–e–d–e" quasi-molecular system of a face of 4D/TSC under time-dependent condensation makes a spiral track, finally reaching the center-of-mass point of the TSC, with a tail of time-varying effective wave length. Electron kinetic energy at $t = 0$ is 19 eV, and it continuously increases during the condensation time (1.4007 fs) reaching finally 57.6 keV at $R_{dd} = 25$ fm. The trapping potential depth of TSC was estimated to be −130.4 keV at $R_{dd} = 25$ fm.

The role and merit of the HMEQPET method for approximating time-dependent TSC trapping potential and relating to the estimation of time-dependent Coulomb barrier penetration probabilities of 4D cluster is explained. HMEQPET provides a practical method for calculating time-dependent (hence time-averaged) fusion rate under TSC condensation, based on Fermi's first golden rule.

2. Condensation motion of 4D/TSC by Langevin equation

The basics of methods with Langevin equations for D-cluster dynamics, especially for D-atom, D_2 molecule, D_2^+ ion, D_3^+ ion, in a 4D/TSC (tetrahedral symmetric condensate) and $6D^{2-}$/OSC (octahedral symmetric condensate) are described in our latest paper [4].

First, one-dimensional Langevin equations for D-clusters with the R_{dd} (d–d distance) are formulated under the Platonic symmetry [2] of multi-particle D-cluster systems with deuterons and quantum-mechanical electron centers. Under the orthogonally coupled Platonic symmetry for a Platonic deuteron system and a Platonic electron system, dynamic equations for so-many-body system of deuterons and electrons with metal atoms, a simple one-dimensional Langevin equation for the inter-nuclear d–d distance R_{dd} can be formulated, as we showed in the previous paper [4]. The Langevin equation of electron-cloud-averaged expectation value of d–d distance R_{dd} for D-cluster is given by

$$N_e m_d \frac{d^2 R}{dt^2} = -\frac{k}{R^2} - N_f \frac{\partial V_s}{\partial R} + f(t). \tag{1}$$

This is the basic Langevin equation for a Platonic symmetric D-cluster having N_e d–d edges and N_f faces of "d–d–e" (D_2^+) or "d–e–d–e" (D_2) type. Here, R is the d–d distance and m_d is the deuteron mass, V_s is the d–d pair trapping potential of either "d–e–d–e"-type ($i = 2$) or "d–d–e"-type ($i = 1$) molecule. The first term on the right side in Eq. (1) is the total Coulomb force (converted to one-dimensional variable R) of the D-cluster system, and $f(t)$ is the fluctuation of force for which we introduce a quantum mechanical fluctuation of deuteron positions under condensation motion. The quantum mechanical effect of electron clouds is incorporated with the second term on the right-hand side as "friction" in Langevin equation. Parameters for different D-clusters are given in Table 1.

Table 1. Parameters of D-cluster Langevin equation.

Cluster	N_e (number of d–d edges)	K (total Coulomb force parameter, keV pm)	Type of electron trapping potential on a surface	N_f (number of faces)
D_2	1	0	$i = 2$	1
D_2^+	1	0	$I = 1$	1
D_3^+	3	6.13	$i = 1$	6
4D/TSC	6	11.85	$i = 2$	6
$6D^{2-}$/OSC	12	29.3	$i = 1$	24

By taking the QM ensemble average with d–d pair wave function, assumed as Gaussian distribution of Eq. (5), we derived the Langevin equation for 4D/TSC as Eq. (2). By taking QM ensemble average of Eq. (3) using Eq. (4), we obtained Eq. (6) for expectation value $\langle R_{dd}\rangle$. We obtained the time-dependent TSC-cluster trapping potential [4] as Eq. (7). The balancing to the Platonic symmetry after distortion (deviation from symmetry) works by the third term of Eq. (7).

$$6m_d\frac{d^2R_{dd}(t)}{dt^2} = -\frac{11.85}{[R_{dd}(t)]^2} - 6\frac{\partial V_{s2}(R_{dd}(t);1,1)}{\partial R_{dd}(t)} + \langle f(t)\rangle + f'(t), \tag{2}$$

$$f'(t) = f(t) - \langle f(t)\rangle, \tag{3}$$

$$f(t) = \left[-\frac{\partial \Delta E_c(R_{dd})}{\partial R_{dd}}\right] \bmod [X^2(R'_{dd};\, R_{dd}(t))], \tag{4}$$

$$X^2(R'_{dd};\, R_{dd}(t)) = \frac{1}{\sqrt{2\pi\sigma^2}}\exp[-(R'_{dd} - R_{dd}(t))^2/(2\sigma^2)], \tag{5}$$

$$6m_d\frac{d^2\langle R_{dd}\rangle}{dt^2} = -\frac{11.85}{\langle R_{dd}\rangle^2} - 6\frac{\partial V_s(\langle R_{dd}\rangle; m, Z)}{\partial\langle R_{dd}\rangle} + 6.6\left\langle\frac{(R' - R_{dd})^2}{R_{dd}^4}\right\rangle, \tag{6}$$

$$V_{TSC}(R' : R_{dd}(t)) = -\frac{11.85}{R_{dd}(t)} + 6V_s(R_{dd}(t); m, Z) + 2.2\frac{|R' - R_{dd}(t)|^3}{[R_{dd}(t)]^4}. \tag{7}$$

A similar Langevin equation and trapping potential were derived for $6D^{2-}$ ion molecule also. We compared the central potential curve (at $R' = R_{dd}$) in Fig. 1. We found that 4D(or H)/TSC can condense ultimately to a very small charge neutral entity and has no stable or ground state. This may be the reason that we do not observe the D_4 molecule in nature. On the contrary, $3D^+$ molecule and $6D^{2-}$ molecule have stable and ground states [4].

Equation (6) was numerically solved by the Verlet method [3], with the result shown in Fig. 2.

Time-dependent barrier penetration probabilities (as a function of R_{dd}, since we have a one-to-one relation between elapsed time and $R_{dd}(t)$) are calculated by HMEQPET method [3] and shown in Table 2.

The fusion rate is calculated by the following Fermi's golden rule [3,4],

$$\lambda_{nd} = \frac{2}{\hbar}\langle W\rangle P_{nd}(r_0) = 3.04\times 10^{21} P_{nd}(r_0)\langle W\rangle. \tag{8}$$

Table 2. Calculated time-dependent (equivalently R_{dd} dependent) barrier factors of 4D/TSC condensation motion.

Elapsed time (fs)	R_{dd} (pm)	P_{2d} (2D barrier factor)	P_{4D} (4D barrier factor)
0	74.1 (D_2 molecule)	1.00E–85	1.00E–170
1.259	21.8 (dde*(2,2); Cooper pair)	1.30E–46	1.69E–92
1.342	10.3	2.16E–32	4.67E–64
1.3805	4.12	9.38E–21	8.79E–41
1.3920	2.06	6.89E–15	4.75E–29
1.3970	1.03	9.69E–11	9.40E–21
1.39805	0.805 (muon-dd molecule)	1.00E–9	1.00E–18
1.39960	0.412	9.40E–7	2.16E–13
1.40027	0.206	3.35E–5	1.12E–9
1.40047	0.103	1.43E–3	2.05E–6
1.40062	0.0412	1.05E–2	1.12E–4
1.40070	0.0206 (TSC-min)	4.44E–2	1.98E–3

Here P_{nd} is the barrier factor for nD-cluster and $\langle W \rangle$ is the averaged value of imaginary part of nuclear optical potential [3,4]. The extrapolation of $\langle W \rangle$ value to 4D fusion was made [3] by using the scaling law $\langle W \rangle \propto (\text{PEF})^5$ with PEF-value which is given in unit of derivative of one pion exchange potential (OPEP) (simple case of Hamada–Johnston potential [4] for pion exchange model. We estimated the next value of 4D fusion yield per TSC generation,

$$\eta_{4d} = 1 - \exp\left(-\int_0^{t_c} \lambda_{4d}(t)\mathrm{d}t\right). \tag{9}$$

Using the time-dependent barrier factors as given in Table 2, we obtained [3] $\eta_{4d} \cong 1.0$. This result means that we have obtained a simple result that 4D fusion may take place with almost 100% yield per a TSC generation, so that macroscopic 4D fusion yield is given simply with a TSC generation rate Q_{TSC} in the experimental conditions of CMNS.

The ultimate condensation is possible only when the double Platonic symmetry of 4D/TSC is kept in its dynamic motion. The sufficient increase (super screening) of barrier factor is also only possible insofar as the Platonic symmetric 4D/TSC system is kept. Therefore, there should be always four deuterons in the barrier penetration and fusion process, so that 4D simultaneous fusion should take place predominantly. The portion of 2D (usual) fusion rate is considered to be negligible [3].

Typical nuclear products of 4D fusion are predicted to be two 23.8 MeV α-particles, although the final state interaction of ^{8}Be* is too complex to be studied yet [5,6].

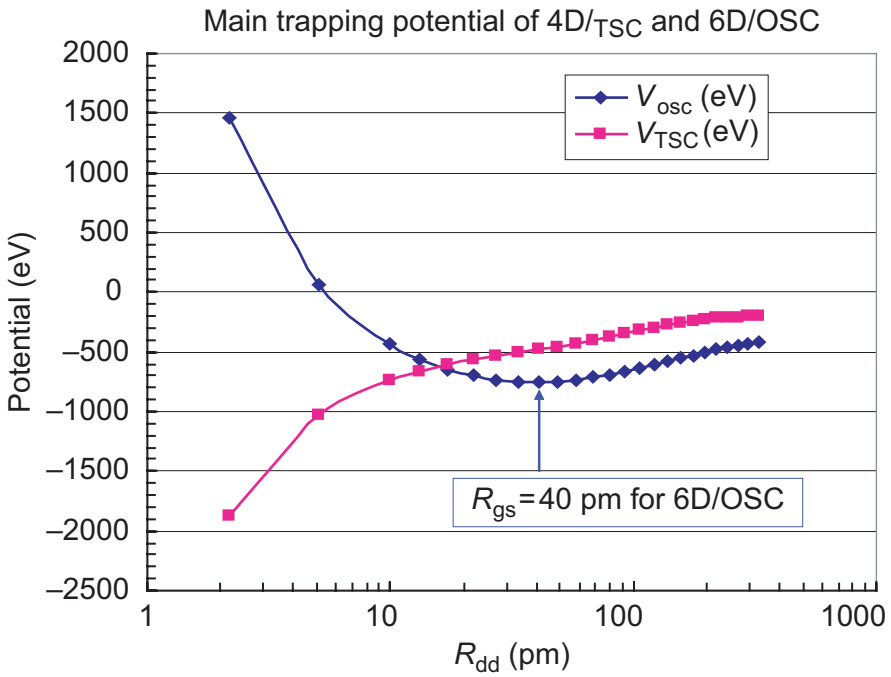

Figure 1. Comparison of cluster trapping potential between 4D/TSC and $6D^{2-}$/OSC. TSC condenses ultimately to very small R_{dd} value (ends at R_{dd-min} = about 20 fm), while OSC converges at R_{dd} = about 40 pm (corresponding to the ground state).

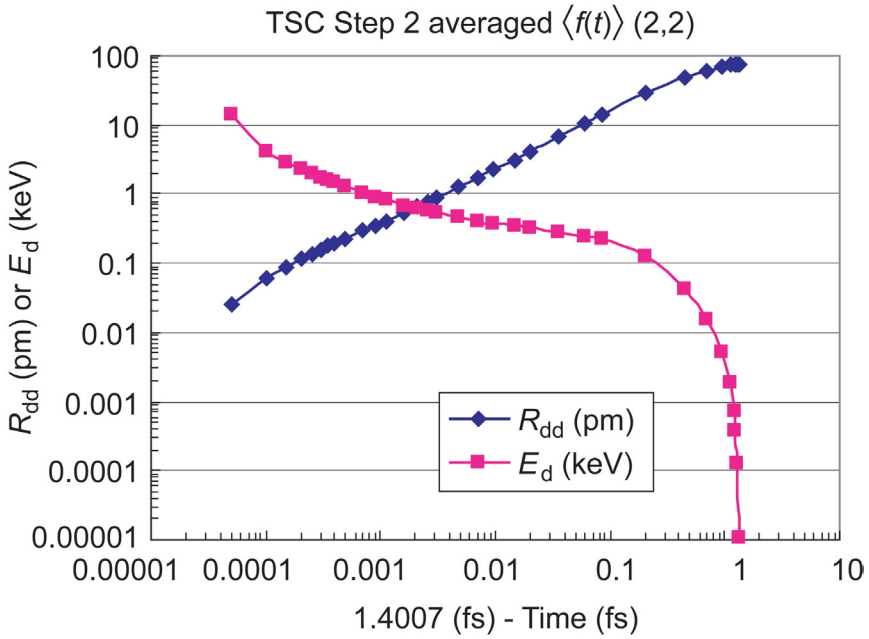

Figure 2. Numerical solution of Eq. (6) by the Verlet method [3]. Time is reversed starting from the condensation time 1.4007 fs.

3. Time-dependent QM behavior of electron clouds

We consider now the dynamic condensation motion of TSC in the view of the Heisenberg uncertainty principle (HUP). In the starting condition of 4D/TSC ($t = 0$), d–d distance R_{dd} was estimated to be the same value (74.1 pm) as that of a

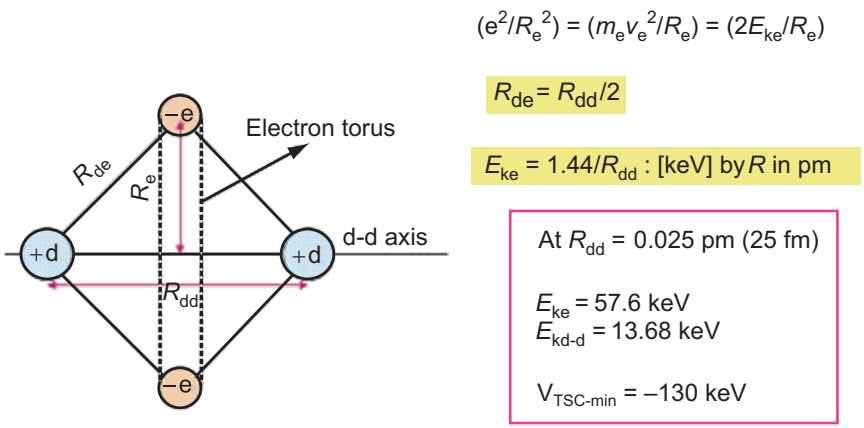

Figure 3. Semi-classical model of "d–e–d–e" EQPET molecule as a face of 4D/TSC (left), and estimated electron kinetic energy at $R_{dd} = 25$ fm (right). Time-dependence of mean electron kinetic energy can be estimated, by assuming the adiabatic quasi-steady state of "d–e–d–e" system in every small time-step.

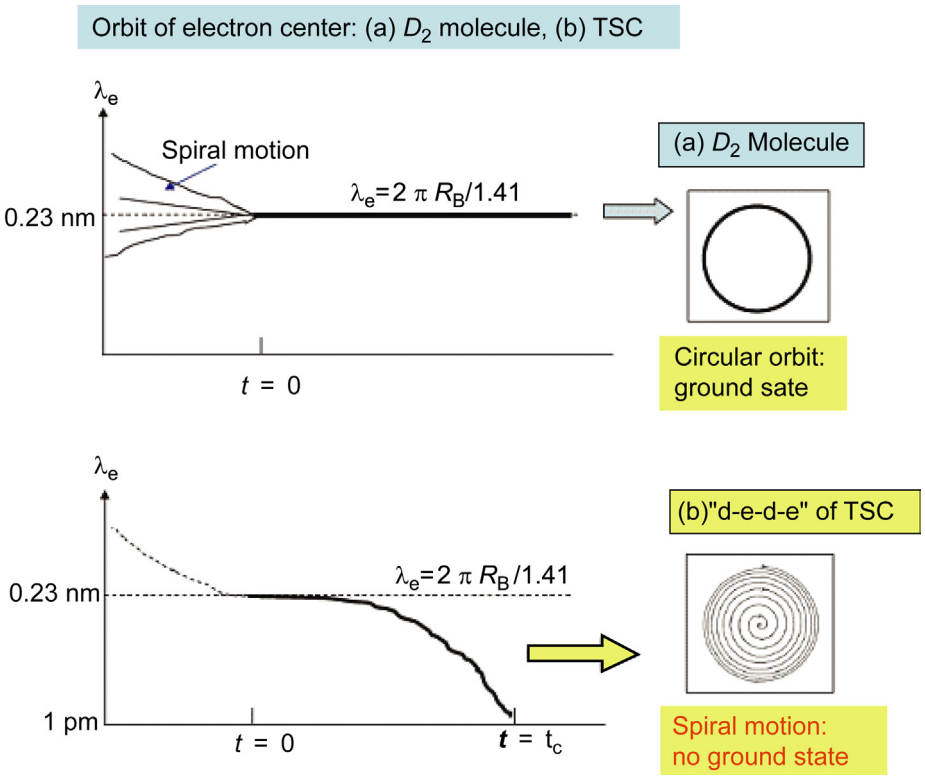

Figure 4. Time-dependent behavior of effective electron wave length: (a) D_2 molecule, (b) "d–e–d–e" EQPET molecule of 4D/TSC.

D_2 molecule. At this starting point, mean electron kinetic energy of one "d–e–d–e" face EQPET molecule out of TSC six faces was 17.6 eV (19 eV by semi-classical model). During the non-linear condensation of TSC, as the parameters given in Table 2 show, the size of "d–e–d–e" EQPET molecule as a face of 4D/TSC decreases from $R_{dd} = 74.1$ pm at $t = 0$ to $R_{dd} = 20.6$ fm at $t = 1.4007$ fs. In the view of HUP, the electron wave length should decrease accordingly to the decrement of R_{dd}. At around $t = 1.4007$ fs, the mean kinetic energy of the electron for a "d–e–d–e" EQPET molecule was estimated [3] to be 57.6 keV. A semi-classical model of "d–e–d–e" EQPET molecule is shown in Fig. 3. This semi-classical model reflects the original Langevin equation for the D_2 molecule, before the quantum-mechanical ensemble averaging is done, as given by,

$$m_d \frac{d^2 R_{dd}}{dt^2} = -(4\sqrt{2} - 2)\frac{e^2}{R_{dd}^2} + \frac{2m_e v_e^2}{(R_{ee}/2)} - \frac{\partial V_{s2}(R_{dd}; 1, 1)}{\partial R_{dd}} + f(t). \tag{10}$$

Here we consider the averaged force-balance between the first term and the second term on the right-hand side of Eq. (10), with ensemble averaging by weight of "adiabatic electron wave function" of modified 1S wave function with decreased de Broglie wave length during every small time step interval.

Considering the relations, $\lambda\!\!\!^{-} = \hbar/mv$ of de Broglie wave length and (kineticenergy) $= (1/2)mv^2$, we understand that the effective quantum mechanical wave length of a trapped electron in TSC has decreased dramatically in the 1.4007 fs condensation time. The estimated trapping potential depth of TSC at around $t = 1.4007$ fs was -130.4 keV.

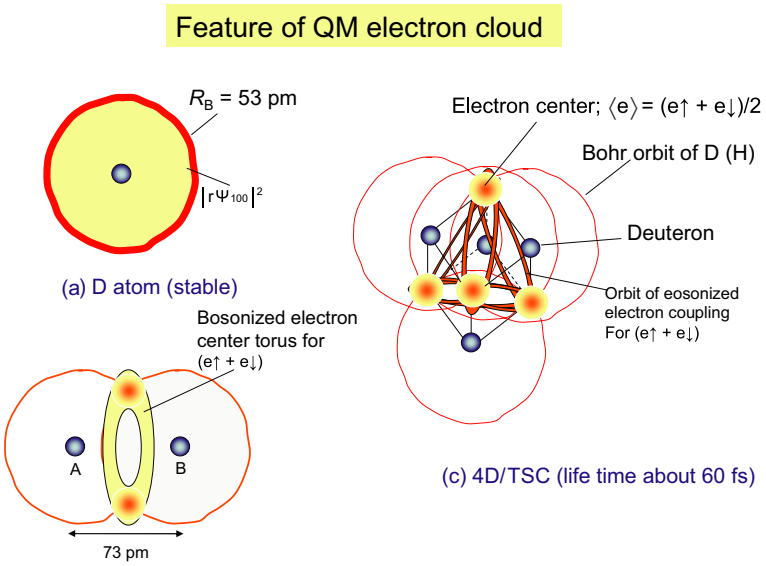

Figure 5. Quantum-mechanical feature of electron clouds for (a) D-atom, (b) D_2 molecule and (c) 4D/TSC ($t = 0$).

This state is understood as an adiabatic state in a very short time interval (about 10^{-20} s) to trap such high kinetic energy (57.6 keV) electrons in very deep (−130.4 keV) trapping potential, to fulfill the HUP condition. By the way, the mean kinetic energy of relative d–d motion was estimated [3] to be 13.68 keV in this adiabatic state, which also diminishes the relative deuteron wave length trapped in the adiabatic TSC potential. In this way, very short R_{dd} (in other words, super screening of mutual Coulomb repulsion) is realized in the dynamic TSC condensation in very fast condensation time ($t_c = 1.4007$ fs) to give, however, a very large 4D simultaneous fusion rate [3,4].

We know that the ground state of the electron orbital (sphere) of D (or H) atom is the Bohr radius ($R_B = 52.9$ pm). The mean kinetic energy of 1S electron is 13.6 eV, the de Broglie wave length of which is 332 pm. And we know $2\pi R_B = 332$ pm to satisfy the continuation of 1S electron wave function by one turn around central deuteron. No other states with a shorter or longer wave length can satisfy the condition of a smooth continuation of wave function, as ground state, for which we must keep the condition that mean centrifugal force equals mean centripetal force.

By the way, quantum mechanical feature of electron clouds are illustrated in Fig. 5, for D-atom, D_2 molecule and 4D/TSC ($t = 0$), respectively.

In contrast to the ground state electron orbital, the electron orbit in a "d–e–d–e" quasi-molecular system makes a spiral track to the center-of-mass point of the TSC, as discussed above. The role and merit of HMEQPET (heavy mass electronic quasi-particle expansion theory) method for approximating time-dependent TSC trapping potential and relating to the estimation of time-dependent Coulomb barrier penetration probabilities of 4D cluster is explained in Section 4.

Similar to the D-atom case, the ground state electron wave function of a D_2 molecule has a steady ground state torus (ring) orbit of two centers of electron clouds [4]. The mean kinetic energy of centrifugal electron motion around the center-of-mass point (middle point of d–d distance) was calculated to be 17.6 eV (19 eV by semi-classical model in Fig. 3), the de Broglie wave length of which is 234 pm and equals $2\pi R_B/1.4142$ to satisfy the smooth continuation of electron wave function along the torus orbit around the center-of-mass point. The dynamic motion of "d-e–d–e"

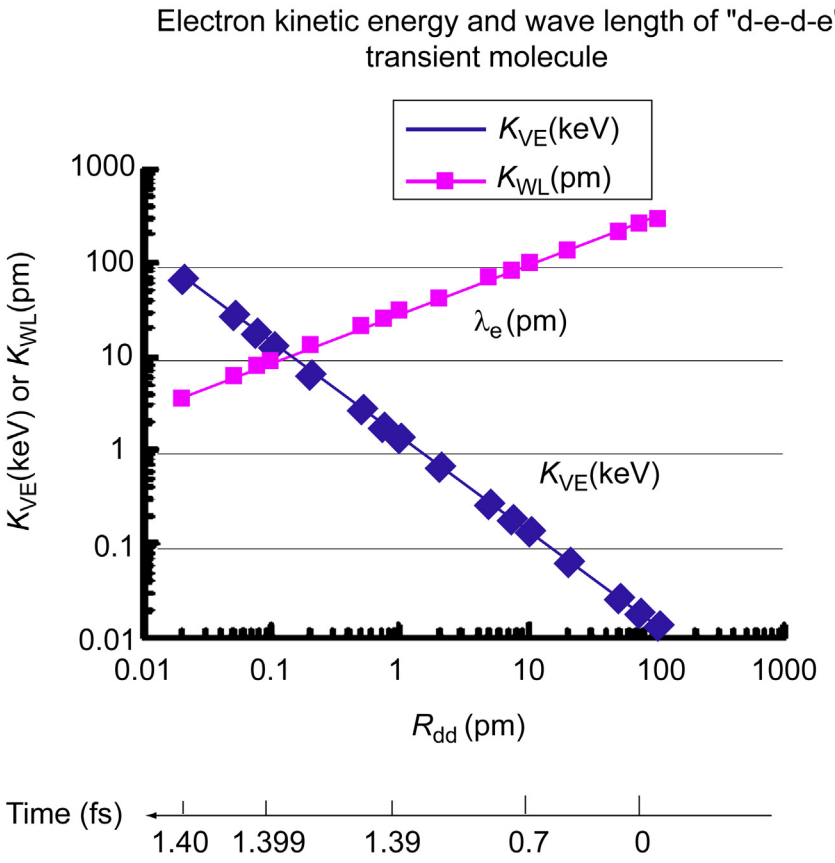

Figure 6. Time variation of mean electron kinetic energy (EKE) and its wave length (EWL) during the 4D/TSC condensation motion in 1.4007 fs condensation time.

four-body system by Langevin equation [Eq. (10)] is illustrated in Fig. 4a. When starting with an arbitrary electron wave length (or momentum), the center of electron cloud follows a spiral orbit to converge finally to the steady torus (ring or circle) orbit with 234 pm one turn length which equals to the ground state effective electron wave length of a D_2 molecule. When we have the strong constraint of TSC trapping potential, the center of the electron cloud follows a spiral orbit time-dependently (Fig. 4b) without a converging ground state. The calculated mean (eigen) energy-values of the D_2 molecule are E_{gs} (ground state system energy) $= -35.1$ eV, E_c (mean Coulomb energy) $= -70.3$ eV, E_{d-d} (mean relative deuteron energy) $= 2.7$ eV and E_{ke} (mean electron kinetic energy) $= 35.2$ eV for two electrons (17.6 eV per electron) [3].

As a result, the centrifugal electron motion in a "d–e–d–e" face follows a spiral curve converging to the central focal point as illustrated in Fig. 4b. If we do not have the strong centripetal Coulombic condensation force by the first term of Eq. (1) right side, for 4D/TSC, the "d–e–d–e" EQPET molecule must go back and converge to the ground state orbit of D_2 molecule, as shown in Fig. 4a.

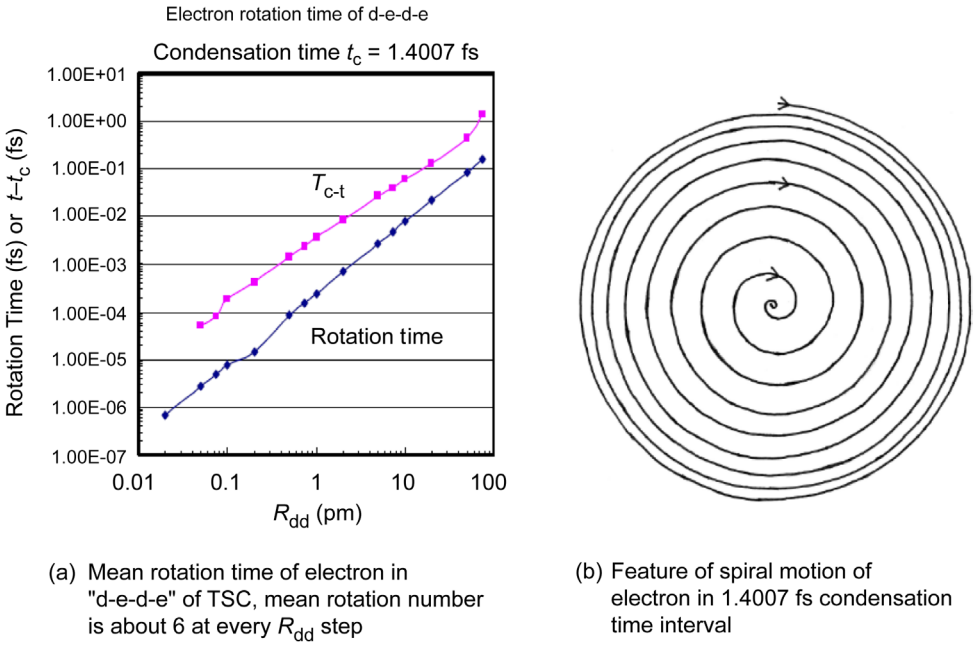

Figure 7. Mean rotation time of electron cloud center under 4D/TSC condensation motion (left) and expanded feature of electron spiral motion (right).

4D/TSC has no steady ground state and the effective electron wave length of a "d–e–d–e" face varies from time to time as illustrated in Figs. 4b and 6.

The spiral motion of the electron center under 4D/TSC condensation is illustrated with expanded scale (right figure), compared with the estimation of mean rotation number of electron in each discrete change of R_{dd} steps, in Fig. 7.

The electron center rotates about six times in each step of R_{dd} changes in Fig. 7. This means the time-dependent electron wave function distributes with a "long" tail along the spiral orbit. This situation does not contradict the Heisenberg uncertainty principle, as a steady ground state does not exist and particles are non-linearly moving.

4. HMEQPET method for fusion rate quantification

The Langevin equation of the expectation value for 4D/TSC and its time-dependent trapping potential are given by Eqs. (6) and (7), respectively. The TSC trapping potential at the final stage (TSC-min) of condensation is shown in Fig. 8.

The depth of the trapping potential is −130.4 keV. The calculated relative kinetic energy of d–d pair is 13.68 keV. In approximation, this potential can be regarded as an adiabatic potential having the d–d pair "quasi-ground state" with $E_{gs} = 13.68$ keV trapped in 130.4 keV deep potential for a very short time-interval of 10^{-20} s. In every time step of the numerical calculation (by the Verlet method [3]), we can draw the approximate adiabatic potential which changes continuously with the change of time.

The kinetic energy of particle is given by $E = (1/2)mv^2$. The de Broglie wave length is given by $\lambda\!\!\!^{-} = \hbar/mv$.

Mean electron kinetic energy increases in a "d–e–d–e" face during condensation motion as shown in Fig. 6. An

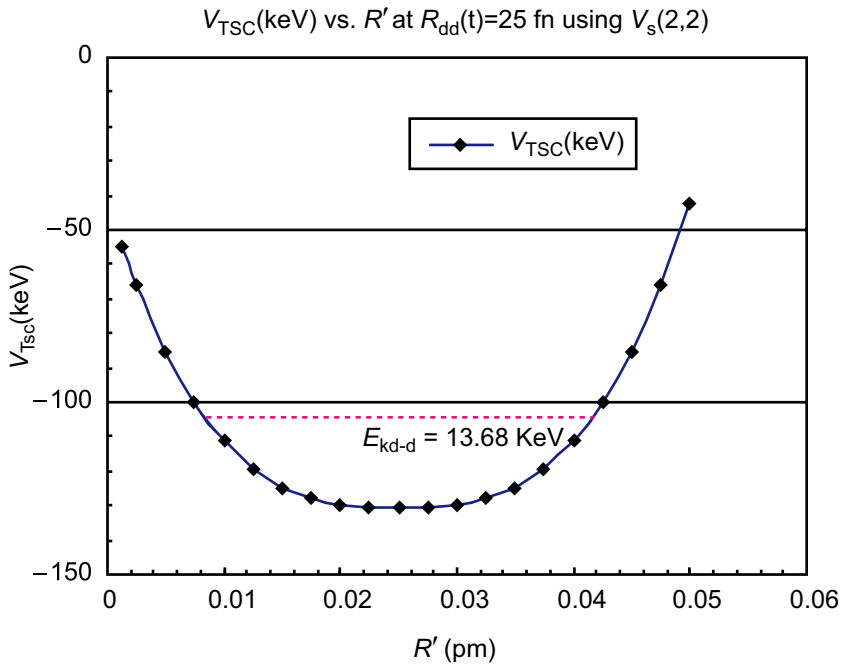

Figure 8. TSC trapping potential at the final stage (TSC-min) of condensation motion by Langevin equation.

electron wave length with increased kinetic energy (or momentum) can be replaced with heavy mass fermion to keep the same "d–e–d–e" size. The HMEQPET method is based on this idea.

From Fig. 3, the mean kinetic energy of an electron in a "d–e–d–e" face is 57.6 keV at $R_{dd} = 25$ fm. A TSC at $t = 0$ has mean electron kinetic energy about 18 eV, the equivalent mass of the "heavy" fermion is estimated to be $\sqrt{57.6 \times 1000/18} = 56.57$ times the electron mass, which is virtual and not the mass of heavy electron in metal physics. The depth of dde*(56.57,2) potential is about −4.8 keV and comparable to the trapping potential of a muonic d–d molecule (see Tables 3 and 2).

Since the depth of 4D/TSC trapping potential at R_{dd}= 25 fm was –130.4 keV, we must assume a much heavier fermion to quantitatively approximate the TSC trapping potential by EQPET dde*(m,Z) potential [1].

We used a Gaussian wave function for d–d pair in Langevin equations. As discussed [3], we cannot use a Gaussian wave function for the estimation of the Coulomb barrier penetration probability (barrier factor), because the tail of the Gaussian function is not accurate enough. Instead, we can use trapping potentials of dde*(m,2) EQPET molecule and Gamow integrals. The assumed quasi-particle state is a heavy Cooper pair e*(m,2) of two "heavy" electrons in a "d–e–d–e" system.

If there exists a one-to-one relation between m and $\langle R_{dd}\rangle(t)$, we can replace all time-dependent TSC trapping potentials with $V_s(R_{dd}(t);m,2)$ potentials of HMEQPET, by continuously adopting a real number of m.

Typical parameters of calculated $V_s(R_{dd}(t);m,2)$ potentials are shown in Table 3. From this table, we derive the following empirical laws:

$$b_0(m, 2) = 0.206 R_{gs}(m, 2), \tag{11}$$

$$m = 9000/b_0(m, 2). \tag{12}$$

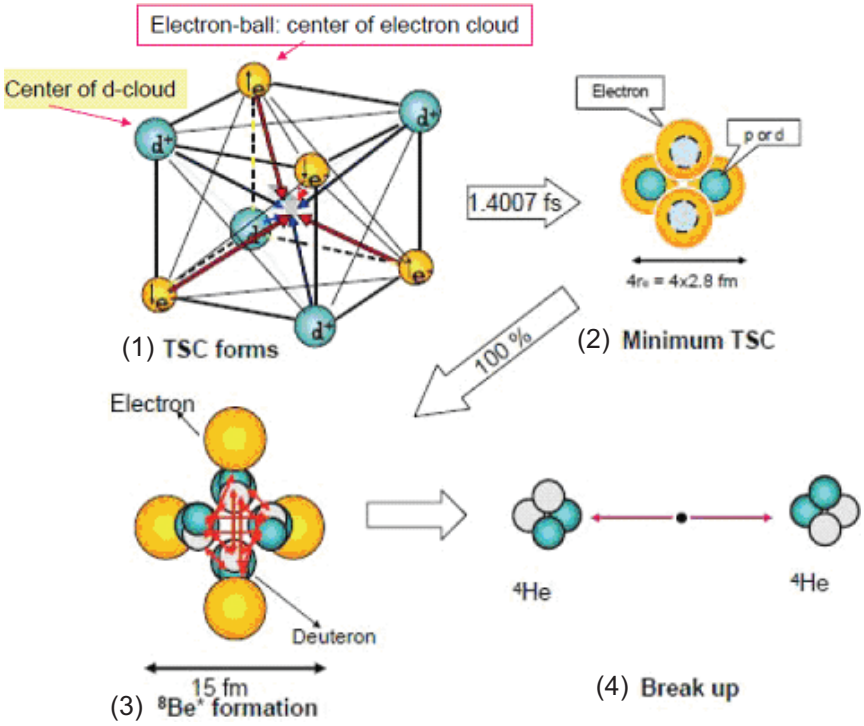

Figure 9. Brief illustration of 4D/TSC condensation motion, in four steps.

Here b_0 and R_{gs} values are given in fm units. Muonic dd-molecule has $R_{gs} = 805$ fm, and $m = 54\,m_e$ of HMEQPET potential corresponds to it. The final stage of TSC potential corresponds to $m = 2000\,m_e$.

Calculated barrier factors by HMEQPET method are already given in Table 2. Finally, we again illustrate the 4D/TSC condensation motion in Fig. 9.

Table 3. Calculated HMEQPET potentials and their parameters. E_{gs}–V_{s-min} gives mean relative kinetic energy of a trapped d–d pair

Molecule	b_0 (pm)	R_{min} (pm)	V_{s-min}(keV)	E_{d-d} (keV)	R_{gs} (pm)	E_{gs} (keV)
D_2	22	70	–0.03782	0.00268	**76.69**	–0.03514
dde* (2,2)	4.5	19.3	–0.1804	0.01013	**21.82**	–0.17027
dde*(5.2)	1.9	7.6	–0 4509	0.0208	**8.72**	–0.43007
dde* (10,2)	0 90	3.8	–0.9019	0.0418	**4.36**	–0.86012
dde* (20,2)	0.45	1.9	–1.8039	0.0837	**2.18**	–1.7202
dde*(50,2)	0.18	0.76	–4.5097	0.2094	**0.873**	–4.3003
dde*(100,2)	0.09	0.38	–9.0194	0.4196	**0.436**	–8.5998
dde* (200,2)	0.045	0.19	–18.039	0.843	**0.218**	–17.196
dde* (500,2)	0.018	0.076	–45.097	2.135	**0.0873**	–42.968
dde*(1000,2)	0.009	0.038	–90.194	4.336	**0.0436**	–85.858
dde* (2000,2)	0.0045	0.019	–180.39	8.984	**0.0218**	–171.406

5. Conclusions

Further explanation of the 4D/TSC condensation motion by quantum-mechanical stochastic differential equations (Langevin equations) has been given in this paper. The electron orbit in a "d–e–d–e" quasi-molecular system of a face of 4D/TSC under time-dependent condensation makes a spiral track finally reaching the center-of-mass point of the TSC, with a tail of time-varying effective wave length. There is found no contradiction with the Heisenberg uncertainty principle.

The role and merit of HMEQPET (heavy mass electronic quasi-particle expansion theory) method for approximating the time-dependent TSC trapping potential and relating to the estimation of time-dependent Coulomb barrier penetration probabilities of 4D cluster is explained.

Dynamics analyses by Langevin equations for D- (or H-) clusters are useful tools to quantitatively estimate the time-dependence of expectation values and trapping potentials, as well as time-dependent fusion rates.

Acknowledgment

The author acknowledges the support of Technova Inc., Tokyo, for this work.

References

[1] A. Takahashi, A theoretical summary of condensed matter nuclear effects, *J. Condensed Matter Nucl. Sci.* **1** (2007) 129–141.
[2] A. Takahashi, N. Yabuuchi, Condensed matter nuclear effects under Platonic symmetry, *Proc. ICCF13*, Sochi, Russia, 2007 (to be published).
[3] A. Takahashi, N. Yabuuchi, Study on 4D/TSC condensation motion by non-liniear Langevin equation, *LENR Source Book, American Chemical Society*, 2007, to be published from Oxford Univ. Press, August 2008.
[4] A. Takahashi, N. Yabuuchi, D-cluster dynamics and fusion rate by Langevin equation, *Proc. 8th Int. Workshop on Anomalies in D/H Loaded Metals*, Catania, Italy, 2007, to be published in 2008.
[5] A. Takahashi, A chronicle of condensed cluster fusion models, *Proc. JCF8*, Kyoto, 2007, pp. 51–62, Japan CF Research Society, 2008.
[6] A. Takahashi, "*Cold Fusion 2008 – mechanism of condensed cluster fusion*" (in Japanese), Kogakusha, Tokyo, 2008.

J. Condensed Matter Nucl. Sci. 2 (2009) 45–50

Research Article

Enhanced Low Energy Fusion Rate in Metal Deuterides Due to Vibrational Deuteron Dipole–Dipole Interactions and Associated Resonant Tunneling Between Neighbouring Sites

J.S. Brown*

Clarendon Laboratory, 1 Parks Rd, Oxford, UK

Abstract

It is observed that interstitial hydrogen nucleii on a metallic lattice are strongly coupled to their near neighbours by the unscreened electromagnetic field mediating transitions between low-lying states. It is shown that the dominant interaction is of dipole–dipole character. By means of numerical calculations based upon published data, it is then shown that in stoichiometric PdD, in which essentially all interstitial sites are occupied by a deuteron, certain specific superpositions of many-site product states exist that are lower in energy than the single-site ground state, suggesting the existence of a new low temperature phase. Finally, the modified behaviour of the two-particle wavefunction at small separations is investigated and prelimary results suggesting a radical narrowing of the effective Coulomb barrier are presented.

Keywords: RDDI, Phase transition, Protons, Deuterons, Metal, Interference, Entanglement, Fusion

PACS: 33.50.-j, 61.72.Ji, 64.70.Kb, 71.35.Lk

1. Introduction

Several metallic elements, notably palladium, vanadium, niobium and nickel, can reversibly absorb hydrogen up to the point of stoichiometry, in which every available interstitial site – of octahedral (O) or tetrahedral (T) symmetry – is occupied by a hydrogen nucleus. A single hydrogen nucleus in such an environment exhibits a spectrum of singlet, doublet and triplet state representations of the local point symmetry group. The ground state is invariably a singlet with even $[+\,+\,+]$ parity along each of the symmetry axes. The next level is, in an fcc lattice, a triplet of states with parities $[-\,+\,+]$, $[+\,-\,+]$, $[+\,+\,-]$ and an excitation energy of the order of 60 meV. The dipole moment between the ground state singlet and the first excited triplet is typically of the order of 0.2 Åe. Since the electronic Fermi gas couples weakly to the electromagnetic field quanta in this part of the spectrum, such a dipole moment gives rise to an

*E-mail: xxx

essentially unscreened resonant dipole–dipole interaction (RDDI) between nearest neighbours [1]. Simple geometrical considerations reveal this to be of the order of 20 meV per pair. Not only is this typically several times larger than screened static Coulomb interaction, it is also manifestly an appreciable fraction of the (on-diagonal) excitation energy of the dipole itself. Since in the quasi-stoichiometric loading regime each hydrogen has several nearest neighbours, it has previously been speculated [2] that there exist many-site states for which the total collective effect of the interaction is a multiple of the pair interaction. This paper sets out to answer the, in our opinion, intriguing question as to whether there exists any such collective state of quantum-entangled dipoles whose total energy is lower than the simple product of ground states, and to obtain an upper bound on the lowest possible energy of such an ensemble of coupled oscillators.

2. Model

The single particle states ψ_n are the solutions of

$$H(r)\psi_n(\mathbf{r}) = \left[\frac{-\hbar^2}{2M_{\mathrm{H}}}\nabla^2 + V(\mathbf{r})\right]\psi_n(\mathbf{r}) = \epsilon_n\psi_n(\mathbf{r}), \tag{1}$$

where $V(r)$ is the periodic potential experienced by an infinitely heavy positive charge with fixed metal core positions. The reader is directed to [3] for a detailed discussion of the derivation of this potential using the DFT procedure. In view of the relatively large mass M_{H} of hydrogen nucleii, the lowest energy solutions will generally be well-localised about local minima in V. These minima will coincide with sites of octahedral or tetrahedral symmetry in cubic lattices and hence the levels ϵ_n are an assortment of singlets, doublets and triplet representations of the cubic point symmetry groups. The static (zero frequency) components of the potential disturbance due to the hydrogen nucleus is subject to a screening law of the approximate (Thomas–Fermi) form

$$V_{\mathrm{HH}}(r) = e^2\frac{\mathrm{e}^{-Kr}}{r}, \tag{2}$$

where K is proportional to the DOS at the Fermi surface.

K is typically much greater than a reciprocal lattice vector. The static Coulomb H–H interaction between nearest neighbours is consequently small, typically not more than a few meV, and essentially state-independent. By contrast, the attenuation of the electromagnetic field due to a transition between levels is negligible over the dimensions of a lattice cell. Since the interparticle interaction is so strongly frequency dependent, the full Hamiltonian cannot be written in closed analytical form. However, matrix elements between pairs of two-site states are simply given by:

$$H_{i_1,j_1;i_2,j_2} = e^2\langle j_1, j_2|\frac{\mathrm{e}^{-K|\mathbf{r}_1-\mathbf{r}_2-\mathbf{R}|\delta(\epsilon_{i_1}-\epsilon_{j_1})\delta(\epsilon_{i_2}-\epsilon_{j_2})}}{|\mathbf{r}_1-\mathbf{r}_2-\mathbf{R}|}|i_1, i_2\rangle, \tag{3}$$

where $\mathbf{R}$ is the intersite displacement vector. The $\delta(\epsilon_i - \epsilon_f)$ factors express the fact that only transitions between different levels give rise to an unscreened interaction.

If just the lowest order term in the multipole expansion of the Coulomb operator $1/|\mathbf{r}_1 - \mathbf{r}_2 - \mathbf{R}|$ is retained, there is no need for double integration over both volumes. In this approximation, (3) reduces to the familiar expression for a dipole–dipole interaction:

$$H_{i_1,j_1;i_2,j_2} \approx \frac{e^2}{R^3}\langle j_1|\mathbf{r}_1|i_1\rangle\cdot\langle j_2|\mathbf{r}_2|i_2\rangle - \frac{3e^2}{R^5}\langle j_1|\mathbf{R}\cdot\mathbf{r}_1|i_1\rangle\langle j_2|\mathbf{R}\cdot\mathbf{r}_2|i_2\rangle. \tag{4}$$

If a classical dipole is located at every interstitial O-site in an fcc lattice, the interaction energy is lowest with the following orientations over a constant-z plaquette:

$$\begin{bmatrix} \leftarrow & \circ & \rightarrow & \circ & \leftarrow & \circ & \rightarrow & \circ & \leftarrow \\ \circ & \uparrow & \circ & \downarrow & \circ & \uparrow & \circ & \downarrow & \circ \\ \rightarrow & \circ & \leftarrow & \circ & \rightarrow & \circ & \leftarrow & \circ & \rightarrow \\ \circ & \downarrow & \circ & \uparrow & \circ & \downarrow & \circ & \uparrow & \circ \\ \leftarrow & \circ & \rightarrow & \circ & \leftarrow & \circ & \rightarrow & \circ & \leftarrow \end{bmatrix}, \tag{5}$$

where the open circles represent the sites of the metal cores at locations [**1 0 0**], [**3 0 0**], [**1 1 1**], etc. It can be shown that there is zero net interaction between parallel layers when each layer has such an arrangement. Guided by this classical analogue, we will limit our search for minimum energy states to those constructed from:

[+ + +] parity states at all O-sites in a $z = 0$ plaquette,
[− + +] parity states at O-sites of even y,
[+ − +] states at O-sites of odd y,
[+ + +] ground states at all sites external to the plaquette.

For the rest of this paper we will use the shorthand $|s, n\rangle$ to denote the nth state of [+ + +] parity, $|p_x, n\rangle$ to denote the nth state of [− + +] parity and $|p_y, n\rangle$ to denote the nth state of [+ − +] parity. The singlet ground state is accordingly written as $|s, 0\rangle$. If the site location needs to be made explicit, we will append this in bold type thus: $|s, 0, \mathbf{110}\rangle$. For clarification, we reproduce below an example of a pair of five-O-site states that are degenerate in zeroth order and that are linked by the dipole–dipole interaction of (4):

$$\begin{bmatrix} |s,0\rangle & \circ & |s,0\rangle \\ \circ & |p_y,0\rangle & \circ \\ |s,0\rangle & \circ & |s,0\rangle \end{bmatrix}, \qquad \begin{bmatrix} |s,0\rangle & \circ & |s,0\rangle \\ \circ & |s,0\rangle & \circ \\ |p_x,0\rangle & \circ & |s,0\rangle \end{bmatrix}.$$

or equivalently:

$$\begin{aligned} &|s,0,\mathbf{000}\rangle \otimes |s,0,\mathbf{020}\rangle \otimes |p_y,0,\mathbf{110}\rangle \otimes |s,0,\mathbf{200}\rangle \otimes |s,0,\mathbf{220}\rangle, \\ &|p_x,0,\mathbf{000}\rangle \otimes |s,0,\mathbf{020}\rangle \otimes |s,0,\mathbf{110}\rangle \otimes |s,0,\mathbf{200}\rangle \otimes |s,0,\mathbf{220}\rangle. \end{aligned} \tag{6}$$

The Hamiltonian matrix in the subspace of the two-O-site states $|s, 0, \mathbf{000}\rangle \otimes |p_y, 0, \mathbf{110}\rangle$ and $|p_x, 0, \mathbf{000}\rangle \otimes |s, 0, \mathbf{110}\rangle$ is, according to (4):

$$\mathbf{H} = \begin{pmatrix} \epsilon_{s,0} + \epsilon_{p,0} & -\frac{3\sqrt{2}e^2d^2}{a^3} \\ -\frac{3\sqrt{2}e^2d^2}{a^3} & \epsilon_{s,0} + \epsilon_{p,0} \end{pmatrix}, \tag{7}$$

where the dipole length $d \equiv \langle s, 0|x|p_x, 0\rangle = \langle s, 0|y|p_y, 0\rangle$. The energy eigenvalues are in this case simply $\epsilon_{s,0} + \epsilon_{p,0} \pm 3\sqrt{2}e^2d^2/a^3$.

More generally, and assuming full hydrogen occupancy and perfect lattice symmetry, the full many-site Hamiltonian matrix depends numerically upon just the lattice parameter a, the dipole lengths d and the energies ϵ of the single-site states.

3. Application to PdD

Quasi-stoichiometric PdH and PdD are natural candidates for our model because the adiabatic effective potential experienced by the hydrogen nucleus has been determined from ab initio DFT calculations [3,4] and the theoretical

spectra found to agree well with IR spectroscopic measurements over a wide range of substoichiometric loading ratios. For this work we checked the results published in [3] by solving (1) on a real-space wedge mesh of pitch 0.03 Å, using the published effective adiabatic Pd-H potential and boundary conditions appropriate to the desired parity. The lattice parameter, corresponding to a displacement like [200] in our notation, is 4.07 Å. The lowest few eigenvectors of the very large sparse matrix were solved using the dominant-diagonal iteration method, as in [5].

The lowest single-site energy levels, relative to the O-site potential, were found to be:

Level	PdH (meV)	PdD (meV)
$\epsilon_{s,0}$	82	52
$\epsilon_{p,0}$	151	95
$\epsilon_{s,1}$	233	149
$\epsilon_{p,1}$	289	186

with the following dipole lengths along each of the three cartesian axes:

Dipole	PdH (Å)	PdD (Å)
$\langle s,0\|x\|p_x,0\rangle$	0.172	0.153
$\langle s,1\|x\|px,0\rangle$	0.128	0.112
$\langle s,0\|x\|px,1\rangle$	−0.003	−0.002
$\langle s,1\|x\|px,1\rangle$	0.194	0.165

Double integration over both site volumes according to (3) yielded the following off-diagonal elements:

$H_{i_1,j_1;i_2,j_2}$	PdH (meV)	PdD (meV)
$\langle s,0,000\|\otimes\langle p_x,0,110\|H\|p_y,0,000\rangle\otimes\|s,0,110\rangle$	−27	−21
$\langle s,0,000\|\otimes\langle p_x,0,110\|H\|p_y,0,000\rangle\otimes\|s,1,110\rangle$	−20	−15
$\langle s,1,000\|\otimes\langle p_x,0,110\|H\|p_y,0,000\rangle\otimes\|s,1,110\rangle$	−15	−11
$\langle s,0,000\|\otimes\langle p_x,1,110\|H\|p_y,0,000\rangle\otimes\|s,1,110\rangle$	−30	−23
$\langle s,0,000\|\otimes\langle p_x,0,200\|H\|p_x,0,000\rangle\otimes\|s,0,200\rangle$	−13	−10
$\langle s,0,000\|\otimes\langle p_x,0,200\|H\|p_x,0,000\rangle\otimes\|s,1,200\rangle$	−9	−7
$\langle s,1,000\|\otimes\langle p_x,0,200\|H\|p_x,0,000\rangle\otimes\|s,1,200\rangle$	−7	−5
$\langle s,0,000\|\otimes\langle p_x,1,200\|H\|p_x,0,000\rangle\otimes\|s,1,200\rangle$	−14	−11
$\langle s,0,000\|\otimes\langle p_x,0,020\|H\|p_x,0,000\rangle\otimes\|s,0,020\rangle$	6	5
$\langle s,0,000\|\otimes\langle p_x,0,020\|H\|p_x,0,000\rangle\otimes\|s,1,020\rangle$	5	4
$\langle s,1,000\|\otimes\langle p_x,0,020\|H\|p_x,0,000\rangle\otimes\|s,1,020\rangle$	4	3
$\langle s,0,000\|\otimes\langle p_x,1,020\|H\|p_x,0,000\rangle\otimes\|s,1,020\rangle$	7	5
$\langle s,0,000\|\otimes\langle p_x,0,220\|H\|p_x,0,000\rangle\otimes\|s,0,220\rangle$	−1	−1
$\langle s,0,000\|\otimes\langle p_x,0,220\|H\|p_x,0,000\rangle\otimes\|s,1,220\rangle$	−1	−1
$\langle s,1,000\|\otimes\langle p_x,0,220\|H\|p_x,0,000\rangle\otimes\|s,1,220\rangle$	−1	−1
$\langle s,0,000\|\otimes\langle p_x,1,220\|H\|p_x,0,000\rangle\otimes\|s,1,220\rangle$	0	−1

3.1. 5-Site states

As an illustrative example, we will calculate the lowest 5-site energy achievable for a given number of $|p,0\rangle$ states. There are just five 5-site states having one $|p,0\rangle$ and $4|s,0\rangle$ states, namely:

$$\left\{\begin{array}{l} |s,0,000\rangle \otimes |s,0,020\rangle \otimes |s,0,110\rangle \otimes |s,0,200\rangle \otimes |p_x,0,220\rangle \\ |s,0,000\rangle \otimes |s,0,020\rangle \otimes |s,0,110\rangle \otimes |p_x,0,200\rangle \otimes |s,0,220\rangle \\ |s,0,000\rangle \otimes |s,0,020\rangle \otimes |p_y,0,110\rangle \otimes |s,0,200\rangle \otimes |s,0,220\rangle \\ |s,0,000\rangle \otimes |p_x,0,020\rangle \otimes |s,0,110\rangle \otimes |s,0,200\rangle \otimes |s,0,220\rangle \\ |p_x,0,000\rangle \otimes |s,0,020\rangle \otimes s,0,110\rangle \otimes |s,0,200\rangle \otimes |s,0,220\rangle \end{array}\right\}. \tag{8}$$

The corresponding Hamiltonian matrix is (in meV):

$$H = \begin{pmatrix} 43 & 5 & -21 & -10 & -1 \\ 5 & 43 & 21 & -1 & -10 \\ -21 & 21 & 43 & 21 & -21 \\ -10 & -1 & 21 & 43 & 5 \\ -1 & -10 & -21 & 5 & 43 \end{pmatrix} + 5\epsilon_{s,0}\mathbf{I}_5, \tag{9}$$

where we have separated out the energy of the conventional ground state. The energy eigenvalues in this small subspace are 3,29,37,59 and 88 meV relative to $5\epsilon_{s,0}$. For the 80 five-site states that comprise just one $|p,0\rangle$ and four $|s,n<2\rangle$ states, the lowest two energy eigenvalues are found to be -2 and 26 meV relative to $5\epsilon_{s,0}$. It is clear from this that the $|s,1\rangle$ states make a significant contribution to the lowest energy eigenvector. In an attempt to find a converged value for the absolute mimimum site energy, Hamiltonian matrices were constructed for a series of plaquettes of increasing size up to a limit set by the memory capacity of our machine. The 15 sites included were: [**0 0 0**], [**0 2 0**], [**1 1 0**], [**2 0 0**], [**2 2 0**], [**1 3 0**], [**3 1 0**], [**3 3 0**], [**4 2 0**], [**1 -1 0**], [**-1 1 0**], [**2 4 0**], [**1 3 0**], [**0 4 0**], [**1 5 0**] , in that order. The results obtained for the energies (E_0, E_1) of the lowest two states relative to $N\epsilon_{s,0}$ are summarized in the following table. For the larger plaquettes, an energy cut-off was applied in order to limit the size of the matrix.

Sites	p-states	Cut-off (meV)	States	E_0 (meV)	E_1 (meV)	E_0 / Site (meV)
5	1	–	80	−2	26	0
5	2	–	80	31	43	6
6	1	–	192	−4	19	−1
6	2	–	240	12	37	2
8	1	–	1024	−15	12	−2
8	2	–	1792	−9	12	−1
9	1	–	2304	−16	9	−2
9	2	300	1044	−14	5	−2
12	1	300	2784	−21	−7	−2
12	2	300	3696	−33	−9	−3
12	3	300	2200	−34	−12	−3
12	4	300	4455	−24	−8	−2
15	2	300	9660	−40	−23	−3
15	3	300	5915	−44	−25	−3
15	4	250	1365	−26	−8	−2

4. Conclusions

The intrinsic complexity of this exact method and the inapplicablity of a perturbative approach have so far confounded our attempts to establish a lower bound on the absolute minimum site energy. It follows from the variational principle that inclusion of higher $|s, n\rangle$ states, as well as further increase in plaquette size, will result in even lower minimum energies. A mean-field approach is perhaps indicated, but we have as yet to find a sufficiently accurate formulation. It is nevertheless already clear from the above data that entangled states are favoured in the stoichiometric regime. The existence of a low temperature phase in which all the deuterons cohere in a mesoscopically entangled state is hence strongly indicated.

5. Over-cancellation of Coulomb barrier

At small interparticle distances: $-K|r_1 - r_2| << 1$, the off-diagonal elements of the type we have been considering are comparable in magnitude, but opposite in sign, to the static Coulomb pair repulsion term. It is hence reasonable so suppose that, once coherence has been established, the height and width of the effective Coulomb barrier between neighbouring s, p state pairs is reduced, with a concommitant increase in the – normally infinitesimally slow – D–D fusion rate. In order to investigate the magnitude of this effect, we solved the two-particle Hamiltonian for the two states discussed in connection with (7) above. Both the static (2) and dynamic (3) interactions were included. Memory constraints limited us to a grid resolution of 0.06 Å. In view of (6) and (7), the solution was constrained to be of the form:

$$\begin{pmatrix} \psi(x_1, y_1, z_1, x_2 - \frac{a}{2}, y_2 - \frac{a}{2}, z_2) \\ -\psi(x_2 - \frac{a}{2}, y_2 - \frac{a}{2}, z_2, y_1, x_1, z_1) \end{pmatrix}, \tag{10}$$

where ψ is odd in its 5th argument and even in all others.

It was found that the lowest energy solution, with

$$\epsilon \approx \epsilon_{s,0} + \epsilon_{p,0} - \frac{3\sqrt{2}e^2d^2}{a^3}, \tag{11}$$

exhibited an increased probability for close encounters of the two hydrogen nucleii right down to the limit of our resolution. At $|r_1 - r_2| = 0.06$ Å, the amplitude was enhanced by about an order of magnitude over the simple product state that pertains when interaction is neglected. This exciting result implies that the dipole–dipole attraction effectively over-cancels the Coulomb repulsion at least down to this length scale. The region of overlap was concentrated about the T-site lattice potential minima that are equidistant between the two O-sites.

6. Further work

A search is currently being undertaken for other metallic lattices with high affinity for hydrogen and flat effective potentials. A multi-level grid DFT algorithm of high accuracy has been developed for this purpose.

References

[1] G. Kurizki, A. Kofman, V. Yudson, *Phys. Rev.* A **53** (1996) R35-–R38.
[2] J. Brown, arxiv.org/abs/cond-mat/0608292.
[3] H. Krimmel, L. Schimmele, C. Elsässer, M. Fähnle, *J. Phys. Condens. Matt.* **6** (1994) 7679-–7704 .
[4] M. Dyer, C. Zhang, A. Alavi, *ChemPhys. Chem.* **6** (2005) 1711-–1715.
[5] M. Puska, R. Nieminen, *Phys. Rev.* B **29** (1984) 5382-–5397.

J. Condensed Matter Nucl. Sci. 2 (2009) 51–59

Research Article

Overcoming the Coulomb Barrier in Cold Fusion

Talbot A. Chubb *
5023 N. 38th St. Arlington, VA 22207, USA

Scott R. Chubb †
903 Frederick St., Apt. 6, Arlington VA, 22204-6611, USA

Abstract

Schwinger pointed out that under some circumstances the Coulomb barrier between paired charged particles is replaced by a correlation factor in a two-body wave function. This paper shows how having two deuterons bound within a common volume having a multiplicity of potential wells can lead to an energy-minimized Schwinger form of wave equation with wave function overlap. Relevance to a situation in which a small number of deuterium atoms is forced into a fully loaded palladium deuteride (PdD) host is discussed.

Keywords: Bloch state ions, Catalytic nuclear fusion, Coherent partitioning, Cold fusion, Ion band state theory

1. Introduction

In conventional nuclear fusion [1], the presence of a Coulomb barrier between interacting nucleons has always prevented nuclear reactions, except at high collisional energy or in the presence of negative muons. Reaction rates between deuterons are calculated by use of the Gamow factor. When the Gamow factor is applied to deuterons at condensed matter temperatures, it forces reaction rates to be much too low to be observable. Nonetheless, Julian Schwinger believed that the Gamow factor models were wrongly applied to cold fusion experiments. He stated, "In the very low energy cold fusion, one deals essentially with a single state, described by a single-wave function, all parts of which are coherent. A separation into two independent, incoherent factors is not possible, and all considerations based on such a factorization are not relevant [2]".

Energy minimization quantum mechanics can be used to model a localized charged particle pair and its response to its internal Coulomb repulsion potential. This response is normally determined by the value of λ_m/a_m, where λ_m is the DeBroglie wavelength and a_m is the Bohr radius of a particle of mass m. When $\lambda_m/a_m << 1$ the energy-minimizing

*E-mail: tchubb@aol.com
†E-mail: chubbscott@aol.com

configuration is that of adjacent, mutually incoherent single-particle wave functions prevented from significant mutual overlap by a Gamow factor. At $\lambda_m/a_m > 1$, the particles are described by a coherent 2-body wave function in which the two particles occupy a common volume of space. The Coulomb repulsion is expressed by a correlation factor that reduces the magnitude of the 2-body wave function at the overlap "point". An example of such a correlated 2-body wave function is the wave function of the spin-paired electrons of the helium atom.

As described by Seitz, the Hylleraas second approximation wave function is

$$\Phi_s = \mathrm{e}^{-\alpha s}(1 + a_1 u + b_1 |\mathbf{r}_{12}|^2),$$

where $s = |\mathbf{r}_1| + |\mathbf{r}_2|$, $t = |\mathbf{r}_1| - |\mathbf{r}_2|$, and $u = |\mathbf{r}_{12}| = |\mathbf{r}_1 - \mathbf{r}_2|$, and α, a_1 and b_1 are the constants determined by energy minimization [3,4]. $\mathbf{r}_1$ and $\mathbf{r}_2$ are the configuration coordinate position vectors that locate the electrons relative to the helium atom center of mass. The $\mathrm{e}^{-\alpha s}$ dependence is spherically symmetric, like the charge distribution around the H atom. The second factor, involving parameters t and u, modulates the 2-electron wave function and produces a downward cusp at zero separation point where t and $\mathbf{r}_{12} \to 0$ can be rewritten as

$$\Phi_s(\mathbf{r}_{\mathrm{cm}}, \mathbf{r}_{12}) = \Psi(\mathbf{r}_{\mathrm{cm}})\, g(\mathbf{r}_{\mathrm{cm}}, \mathbf{r}_{12}),$$

where $\Psi(\mathbf{r}_{\mathrm{cm}}) = \mathrm{e}^{-2\alpha|\mathbf{r}_{\mathrm{cm}}|}$ and $g(\mathbf{r}_{\mathrm{cm}}, \mathbf{r}_{12}) = \sim 1 + a_1|\mathbf{r}_{12}| + b_1|\mathbf{r}_{12}|^2$.

The $g(\mathbf{r}_{\mathrm{cm}}, \mathbf{r}_{12})$ is a correlation function which describes the anti-correlation between electrons. The amplitude of $\Phi_s(\mathbf{r}_{\mathrm{cm}}, \mathbf{r}_{12})$ decreases where $\mathbf{r}_{12} \to 0$.

Ion band state theory considers systems in which delocalized D^+ ions are embedded in a metal lattice. The dimension scale of the lattice periodicity is set by the electron Bohr radius a_e. The deuteron λ_m is about 1/4000 λ_e, where λ_e is the electron DeBroglie wave length. Since λ_m / a_e is $\sim 1/4000 << 1$, the expectation is that the Gamow factor type wave function would apply. The Schwinger statement contradicts this expectation. He implies that a system supporting cold fusion has been specially prepared so as to make the correlation form of interaction applicable at $\lambda_m/a_m = \sim 1/4000$.

This paper describes how the imposition of lattice periodic order on a D^+ 2-body wave function describing deuterons in a periodic metal lattice can prepare a system so as to satisfy the Schwinger prescription.

2. Density distributions

Function $|\Phi_s|^2$ is the normalized-to-unity density distribution of the 2-electron pair of the ground state helium atom. It is the stationary state distribution referred to in chemistry as a closed-shell orbital. $2e|\Phi_s|^2$ is the charge distribution that neutralizes the nucleus of the helium atom. A more compact electron charge distribution $2e|\Phi_{\mathrm{e,Li}}|^2$ of the same type screens the nucleus of the Li atom. The screened nucleus charge of the lithium atom forms the potential well within which the valence electron is embedded. The Li nucleus screened by $2e|\Phi_{\mathrm{e,Li}}|^2$ is called a mean field distribution in the language of condensed matter physics. The valence electron is prevented from assuming the electron density distribution $|\Phi_{\mathrm{e,Li}}|^2$ by the Pauli exclusion principle.

Figure 1a shows the charge density distribution for the pair of mutually incoherent deuterons of the D_2 molecule. Figure 1b is a similar drawing showing the charge distribution for a pair of coherently connected Bloch function deuterons as envisioned by the Ion Band State Theory [5]. The spatial distribution of a Bloch particle is defined by $|\Psi(r)|^2$, where $|\Psi(r) + \mathbf{R}_j| = |\Psi(r)|$, where $\mathbf{R}_j$ is any of N_{cell} Bravais lattice vectors identifying equivalent locations in the N_{cell} unit cells making up the occupied coherent volume. The coherent deuterons are mixed by imposition of coordinate exchange symmetry. In Fig. 1b, the pictorial representation of the exchange-symmetrized single-particle Bloch deuterons that make up the Bloch D^+ pair are assumed to have identical single-particle wave functions. The charge distribution in Fig. 1b then also describes the charge distribution of each of the single-particle Bloch deuterons.

Figure 1b drawing depicts the density distribution of surface deuterons in contact with a metal surface. The deuterons occupy a volume 1 layer thick and conform to the 2-dimensional array symmetry of the underlying metal

surface. Alternatively, the drawing serves to illustrate the density distribution of Bloch ions occupying a set of interstitial potential wells within a bulk metal crystallite. In either case the volume of the coherently occupied array is finite and measured by counting the number of occupied unit cells N_{cell}. The stationary state single-particle charge density in each potential well is $e|\Psi(r)|^2/N_{\text{cell}}$, assuming one potential well per unit cell.

In this paper the Ion Band State Theory models low-density deuterium matter as delocalized ions embedded in a metal crystallite. It is the "ion" equivalent of the electron band state theory of a metal. The term "ion" is used loosely in that it is required that the ion and the metal's neutralizing electronic charge maintain charge neutrality over the volume of each unit cell of a metal crystallite. Neutralized ions of this type are said to be "dressed". Dressed ions are ions that are fully screened within the confines of a single unit cell volume by the mobile electron medium of the metal. Consider a bulk metal containing numbers of 3-dimensional crystallite volumes separated from each other by potential barriers or by regions of lower crystalline order. Examples of such isolated ordered regions are shown in electron microscope pictures of "atom clusters" by Fujita [7]. We model sets of coherent ions confined to a bounded small local region of relatively high crystalline order. The size of a host crystallites containing a set of ion band state occupations is measured by counting the number of unit cells N_{cell} making up the ion coherence volume.

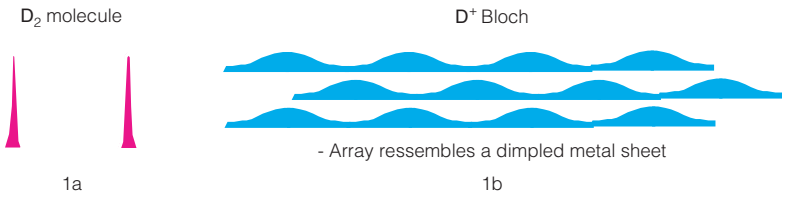

Figure 1. Toy Models: Part a shows the charge distribution of two D^+ in separated potential wells within a molecule's electron cloud. The deuterons are mutually incoherent. The Leggett and Baym modeling [6] has incoherence of this type. Part b shows a single Bloch D^+ in an array of potential wells provided by a metal crystal. Neutralization is provided by the metal's mobile electrons. Localized charge maxima are coherently coupled so that the sum over N_{cell} unit cells is a single delocalized deuteron. Part b can also depict the center-of-mass charge distribution of two Bloch D^+ ions coherently coupled by coordinate exchange, and also of a quasiparticle pairing of Bloch deuterons in a many-body D^+ Bloch system. The array of charge maxima is used to illustrate both a D^+ charge distribution having 3-dimensional periodic symmetry inside a metal, and a D^+ charge distribution inside an interface layer resting on metal surface having 2-dimensional periodic symmetry.

3. 2-Body Bloch function physics

The appropriateness of Fig. 2b Bloch function configuration is determined by energy minimization. Consider the effect of periodic symmetry on the behavior of a coherent many-body D^+ ion system in which a low number-density set of deuterons is subjected to an imposed periodic potential. Consider N_{D} deuterons inside a small crystal consisting of N_{cell} identical unit cells where $N_{\text{D}}/N_{\text{cell}} << 1$. An example would be 100 deuterons in a crystal made up 10^6 unit cells. Such a system is composed of bosons of mass m_{D} and charge e, where m_{D} is the deuteron mass and e is the deuteron charge. The N_{D} deuterons are indistinguishable particles described by single-particle Bloch wave functions $\Psi(\mathbf{r}, \mathbf{k})$ such that $|\Psi(\mathbf{r} + \mathbf{R}_n, \mathbf{k})| = |\Psi(\mathbf{r}, \mathbf{k})|$, where $\mathbf{k}$ is a wave vector quantum index and where the $\mathbf{R}_n$ is a set of N_{cell} distinct Bravais lattice vectors. Each of the set of $\Psi(\mathbf{r}, \mathbf{k})$ has a distribution within physical space $\{\mathbf{r}\}$ with an identical local density maximum in each of the N_{cell} identical unit cells. The energies of the $\Psi(\mathbf{r}, \mathbf{k})$ can be different, but because the D^+ are bosons, they can all be the same. Members of the Bloch D^+ set are allowed to have somewhat different spatial distributions.

The above system is described by a many-body wave function with coordinate exchange. Exchange replaces the N_D single-particle wave functions with N_D single-quasiparticle wave functions described by N_D Bloch functions. Because of exchange symmetry the quasiparticle states are coordinate-entangled. This means that the phase difference between a given pair of quasiparticles remains constant and independent of $\mathbf{r}$. In our treatment of the many-body description we consider only the set of 2-quasiparticle entanglements, one for each of the $N_b(N_b-1)/2$ distinct quasiparticle pairs. A full many-body treatment of the system would include the entanglements between sets of three quasiparticles, sets of four quasiparticles, etc. in addition to the set of paired quasiparticles considered here.

The standard protocol for constructing 2-particle wave functions is to start with a product of single-particle wave functions. This form of wave function gives the correct behavior for particle pairs with no self-interaction [8]. The single-particle wave functions are solutions of a Schrodinger equation. The solutions obtained customarily fit Born Von Karman periodic boundary conditions that do not properly match the box-like boundary that encloses a crystallite volume. In practice this procedure gives useful wave functions when applied to not-too-small lattice volumes. Finite cluster and thin-film calculations involving 3d and 4d metal atoms have shown that the resulting wave functions provide a good description of an embedded system provided that the host bulk-like crystal periodic environment has dimensions more that a few unit cells in depth.

For a periodic potential of the form $U(\mathbf{r}+\mathbf{R}_n)=U(\mathbf{r})$, the eigenstate wave functions are Bloch functions $\Psi(\mathbf{r})$ having "Bloch" symmetry as described by $|\Psi(\mathbf{r}+\mathbf{R}_n)|=|\Psi(\mathbf{r})|$. The simplest 2-body wave function $\Psi(\mathbf{r}_1,\mathbf{r}_2)$ is

$$\Psi(\mathbf{r}_1,\mathbf{r}_2)=\Psi_1(\mathbf{r}_1)\Psi_2(\mathbf{r}_2), \tag{1}$$

where $\Psi_1(\mathbf{r}_1)$ and $\Psi_2(\mathbf{r}_2)$ are single-particle (or single-quasiparticle) Bloch functions and $\mathbf{r}_1$ and $\mathbf{r}_2$ are the physical positions of particles 1 and 2 in the metal lattice. The $\mathbf{r}_1$ and $\mathbf{r}_2$ are configuration coordinate vectors. Atomic physics has shown that this simple form of 2-body wave function is suitable only for modeling distinguishable, mutually incoherent particles 1 and 2. Neglecting the effects of spin, if the particles are indistinguishable and in the same state, the allowed 2-body wave function must have coordinate exchange symmetry, which is symmetric for bosons and suitably paired fermions, and is anti-symmetric for single fermions. Bosons and spin-paired fermions are symmetrized by applying the symmetric coordinate exchange symmetry constraint.

In the Ion Band State Theory, Ψ_1 and Ψ_2 are assumed to be independent Bloch functions and $\mathbf{r}_1$ and $\mathbf{r}_2$ refer to positions $\mathbf{r}$ in the lattice. Functions $\Psi_1(\mathbf{r})$ and $\Psi_2(\mathbf{r})$ have the symmetries:

$$|\Psi_1(\mathbf{r}_1+\mathbf{R}_{1_n})|=|\Psi_1(\mathbf{r}_2)| \quad \text{and} \quad |\Psi_2(\mathbf{r}_2+\mathbf{R}_{2_m})|=|\Psi_2(\mathbf{r}_2)|,$$

where $\mathbf{R}_{1_n}$ and $\mathbf{R}_{2_m}$ are independent Bravais lattice vectors. The 2-body wave function $\Psi(\mathbf{r}_1,\mathbf{r}_2)$ has the dual symmetry

$$|\Psi[(\mathbf{r}_1+\mathbf{R}_{1_n}),\mathbf{r}_2]|=|\Psi(\mathbf{r}_1,\mathbf{r}_2)| \quad \text{and} \quad |\Psi[\mathbf{r}_1,(\mathbf{r}_2+\mathbf{R}_{2_m})]|=|\Psi(\mathbf{r}_1,\mathbf{r}_2)|$$

for all positions $\mathbf{r}$ in the lattice, including the center-of-mass position $\mathbf{r}=\mathbf{r}_{cm}=(\mathbf{r}_1+\mathbf{r}_2)/2$.

4. The double Bloch function self-interaction picture

In order to quantify the point-particle aspect of the Coulombic self-interaction in a 2-body system, it is necessary to express the wave function in terms of center-of mass, separation coordinates, where $\mathbf{r}_{cm}=(\mathbf{r}_1+\mathbf{r}_2)/2$ and $\mathbf{r}_{12}=\mathbf{r}_1-\mathbf{r}_2$. One then seeks 2-body wave function solutions of the appropriate wave equation in terms of separable functions $\Psi(\mathbf{r}_{cm})$ and $g(\mathbf{r}_{12})$. Since $\Psi(\mathbf{r}_1,\mathbf{r}_2)$ is Bloch symmetric with respect to both $\mathbf{r}_1$ and $\mathbf{r}_2$, it is also Bloch symmetric in terms of $\mathbf{r}_{cm}$. The interesting question is the behavior of $\Psi(\mathbf{r}_1,\mathbf{r}_2)$ when $\mathbf{R}_{1_n}$ varies independently of $\mathbf{R}_{2_m}$. The assumption of independent lattice vectors means that $\mathbf{R}_{1_n}-\mathbf{R}_{2_m}=\mathbf{R}_{12_j}$ is also a Bravais lattice vector. This assumption makes $\Psi(\mathbf{r}_1,\mathbf{r}_2)$ Bloch symmetric with respect to both $\mathbf{r}_{12}$ and $\mathbf{r}_{cm}$.

The Schrodinger-like wave equation describing two interacting band state deuterons in a periodic lattice of N_{cell} unit cells is a six degree-of-freedom equation in center-of-mass,separation space. We examine solutions to Eq. (2) of the form

$$\Phi(\mathbf{r}_{\text{cm}}, \mathbf{r}_{12}) = \Psi(\mathbf{r}_{\text{cm}}) g(\mathbf{r}_{12}), \tag{2}$$

where $|\Psi(\mathbf{r}_{\text{cm}}+\mathbf{R}_{\text{cm}})| = |\Psi(\mathbf{r}_{\text{cm}})|$ with $\mathbf{R}_{\text{cm}} = (\mathbf{R}_{1_n}+\mathbf{R}_{2_m})/2$ and $|g(\mathbf{r}_{12}+\mathbf{R}_{12})| = |g(\mathbf{r}_{12})|$ with $\mathbf{R}_{12} = \mathbf{R}_{1_n}-\mathbf{R}_{2_m} \neq 0$ except in one unit cell.

Here $\mathbf{R}_{\text{cm}}$ is a Bravais lattice vector in physical space $\{\mathbf{r}_{\text{cm}}\}$ and $\mathbf{R}_{12}$ is a Bravais lattice vector in separation parameter space $\{\mathbf{r}_{12}\}$. This resulting symmetry is called "double Bloch symmetry". We determine the conditions for which this form of wave function minimizes system energy.

The 2-body wave equation can be separated into two wave equations:

$$\int^{\text{D}^+ \text{ Coherent Vol}} \Psi^*(\mathbf{r}_{\text{cm}}) \left\{ -\frac{\hbar^2}{4m_{\text{D}}} \nabla_{\text{cm}^2} + (2e) U_{\text{lattice}}(\mathbf{r}_{\text{cm}}) \right\} \Psi(\mathbf{r}_{\text{cm}})\, \text{d}^3\mathbf{r}_{\text{cm}} = E_{\text{ext}} \Psi(\mathbf{r}_{\text{cm}}) \tag{3}$$

and

$$\int^{\mathbf{r}_{12} \text{ lattice}} \left\{ -\frac{\hbar^2}{2m_{\text{D}}} \nabla_{12}^2 + \sum_{\substack{j=1 \\ \text{coherent} \\ \text{volume}}}^{N_{\text{cell}}} e^2/(N_{\text{cell}}|(\mathbf{r}_{12} + \mathbf{R}_{12_j})|) \right\} g(\mathbf{r}_{12})\, \text{d}^3\mathbf{r}_{12} = E_{\text{int}}\, g(\mathbf{r}_{12}). \tag{4}$$

The first term in Eq. (3) describes the center-of-mass kinetic energy density of a double deuteron, i.e., a mass-4, charge-2 exchange-symmetrized Bloch quasiparticle, coherently delocalized over N_{cell} unit cells of center-of-mass space. Center-of-mass space $\{\mathbf{r}_{\text{cm}}\}$ is also metal lattice space $\{\mathbf{r}\}$. The second term describes the potential energy of a mass-4, charge-2 exchange-symmetrized Bloch quasiparticle over N_{cell} unit cells of metal lattice space. This potential energy is periodic in physical space. The first term in Eq. (4) describes the kinetic energy density of internal motion of the double deuteron particle over the N_{cell} unit cells of separation space, which is an internal coordinate space associated with the difference in positions of two interacting deuterium nuclei. The second term in Eq. (4) is actually a sum over terms, as shown in Eq. (4). This sum of terms is a function that is well-defined near its singular points, where it describes the $e^2/|r_{12}|$ singular potential of the partitioned double-deuteron's dressed Coulombic self-interaction. Position vector $\mathbf{r}_{\text{cm}}$ ranges over N_{cell} unit cells of $\{\mathbf{r}_{\text{cm}}\}$, and separation vector $\mathbf{r}_{12}$ ranges over N_{cell} unit cells of $\{\mathbf{r}_{12}\}$. $\mathbf{R}_{12_j}$ is a set of N_{cell} Bravais lattice vectors locating equivalent points in $\{\mathbf{r}_{12}\}$.

Figure 2 shows a sketch of a possible $\Psi(\mathbf{r}_{\text{cm}}, \mathbf{r}_{12})$. Wave function factor $\Psi(\mathbf{r}_{\text{cm}})$ shows a density maximum within each of N_{cell} equivalent potential wells provided by lattice potential U_{lattice}. Wave function factor $g(\mathbf{r}_{12})$ causes $|\Psi(\mathbf{r}_{\text{cm}}, \mathbf{r}_{12})|$ to have a local minimum at each $\mathbf{r}_{12} + \mathbf{R}_{12_j} = 0$ point in separation space (i.e., at $\mathbf{r}_{12} = 0$ modulo $\mathbf{R}_{12_j}$). The functional form of $g(\mathbf{r}_{12})$ is that of a near constant amplitude function reduced periodically by a set of N_{cell} cusps. At each cusp point in wave equation (4), a singularity in the partitioned Coulomb self-interaction is cancelled by a singularity in the internal kinetic energy established by a discontinuity in the momentum $(i\hbar/m)\nabla_{12}\, g(\mathbf{r}_{12})$. If the mean value of $g(\mathbf{r}_{12})$ is a and the cusp depth is b, then $(a - b)/a$ is a measure of the degree of D^+D^+ wave function overlap.

5. Energy-minimization

Equation (2) describes band state ions in a metal lattice where a fermi sea of electrons is present that provides ion screening sufficient to guarantee charge neutrality in each unit cell. The electron screening requirement means that the

$e^2/|r_{12}|$ form of the Coulombic interaction shown in Eq. (4) is valid only well inside a screening volume V_{sc}, which is smaller than the volume of the unit cell.

We examine an energy-minimized form of $\Phi(\mathbf{r}_{cm}, \mathbf{r}_{12})$ at large N_{cell} with electron screening included. Energy minimization of Eqs. (3) and (4) proceeds independently. The energy minimized form of Eq. (3) is that of a charge-2, mass-4 double-deuteron in the lattice field $U_{lattice}(\mathbf{r})$. To obtain an energy minimized solution to Eq. (4), we start with a set of trial correlation functions $g(\mathbf{r}_{12})$. Here Hylleraas provides guidance in his approximate solutions for the 2-electron wave function of the helium ground state atom. In analogy to the simplest Hylleraas approximation, we choose a periodic form of Hylleraas-like trial functions $g(\mathbf{r}_{12})$ which meets the lattice requirement for periodic symmetry, namely

$$\begin{aligned} g(\mathbf{r}_{12}) &= A[1 + b\sin(\pi|\mathbf{r}_{12}|/4r_{sc})]/(1+b), && |\mathbf{r}_{12}| < 2r_{sc}, \\ g(\mathbf{r}_{12}) &= g(2r_{sc})A, && |\mathbf{r}_{12}| > 2r_{sc}, \end{aligned} \tag{5}$$

where A is a normalizing constant, b is the depth of the assumed cusp, and r_{sc} is a screening radius beyond which the Coulomb repulsion force between the coupled dressed deuterons is not felt. In the energy minimization process using Eq. (4), N_{cell} is kept fixed and various values of b are chosen so as to minimize the sum of internal potential energy E_{pot} and internal kinetic energy E_{ke}. The normalizing constant A for $g(\mathbf{r}_{12})$ is calculated to be

$$A = \{[1/(1-2b)]^{1/2}\}/(N_{cell}V_{cell}) + O(b^2, r_{sc}^3/V_{cell})$$

with b and r_{sc}^3/V_{cell} treated as small quantities.

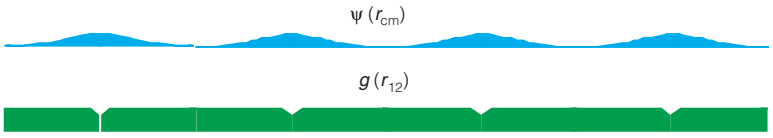

Figure 2. Toy Model. Factor $e|\Psi(\mathbf{r}_{cm})|^2$ measures the charge distribution of 2-D^+_{Bloch} in center-of-mass space $\{\mathbf{r}_{cm}\}$, which is also lattice space. The density distribution is the same array as differently depicted in Fig. 1 b. $g(\mathbf{r}_{12})$ is a Bloch wave function in separation space $\{\mathbf{r}_{12}\}$. It is normalized to a mean value = 1, so as to appear as a correlation function in the 2-body wave function $\Psi(\mathbf{r}_{cm}, \mathbf{r}_{12})$ describing a 2-D^+ Bloch pair. The deuterons are anti-correlated in the sense that the amplitude of $\Psi(\mathbf{r}_{cm}, \mathbf{r}_{12})$ decreases as $\mathbf{r}_{12} \to 0$ modulo $\mathbf{R}_{12_j}$, where $\mathbf{R}_{12_j}$ is a lattice vector in $\{\mathbf{r}_{12}\}$.

6. Cusp depth vs. N_{cell}

The above process determines the value of N_{cell} that minimizes system energy for suitable pre-selected values of b and r_{sc}. We are concerned with the behavior of E_{ke} and E_{pot} at large N_{cell}, for which the value of b that minimizes total energy is much less than 1. How are the $g(\mathbf{r}_{12})$ dependencies of E_{ke} and E_{pot} affected by N_{cell}? In the limit that $b \to 0$, one finds that $A \to 1/(N_{cell}V_{cell})$ and the integrand of the potential energy term $\to (1-2b)\{1+2b\sin(\pi|\mathbf{r}_{12}|/(4r_{sc}))\}$. Then, in the integration of $\mathbf{r}_{12}$ over the N_{cell} unit cells in $\{\mathbf{r}_{12}\}$, we find that

$$E_{ke}(g) = 2\pi(\pi^2/6 - 1)e^2 m_e a_e r_{sc} b^2/(m_D N_{cell} V_{cell}), \tag{6a}$$

where a_e is the electron Bohr radius. Similarly, we find, after integrating over $\mathbf{r}_{12}$, that

$$E_{pot}(g) = -(128/\pi)(\pi^2/8 - 1)r_{sc}\, e^2 b/(N_{cell}^2 V_{cell}). \tag{6b}$$

Evaluating Eq. (8) for an assumed test case, we take $V_{\text{cell}} = 16\,\text{Å}^3$ and $r_{sc} = 0.156\,\text{Å} = 0.1\times$ Wigner Seitz radius. Then

$$E_{\text{ke}}(g) = 0.82 \times 10^{-4} b^2/N_{\text{cell}}\,\text{eV},$$
$$E_{\text{pot}}(g) = -0.224 b/N_{\text{cell}}^2\,\text{eV}.$$

The energy minimizing condition $-\delta E_{\text{pot}}(g)/\delta b = \delta E_{\text{ke}}(g)/\delta b$, occurs at

$$N_{\text{cell}} = (m_{\text{D}}/m_{\text{e}})(r_{sc}/a_{\text{e}})32/\pi^2)[(\pi^2/8-1)/(\pi^2/6-1)](1/b) \quad (7)$$
$$= 0.59(m_{\text{D}}/m_{\text{e}})(r_{sc}/a_0)(1/b).$$

The energy minimizing condition is $N_{\text{cell}} = 6.83 \times 10^2/b$. More than ~90% dd overlap exists at $N_{\text{cell}} \geq 6.8 \times 10^3$, since $b < 0.1$.

Equation (7) shows how cusp amplitude b increases with decreasing N_{cell}. Figure 3 depicts $g(\mathbf{r}_{12})$ at three values of N_{cell}. When b becomes large enough that $g(\mathbf{r}_{12}) \to 0$ at $\mathbf{r}_{12} = 0$ modulo $\mathbf{R}_{12_j}$, the double Bloch wave function model becomes unphysical. Then $\Phi(\mathbf{r}_{\text{cm}}, \mathbf{r}_{12})$ reverts to the molecular form shown in Fig. 1a, and the two D^+ become mutually incoherent. The smallest N_{cell} supporting the Schwinger form of wave equation is designated $N_{\text{cell,critical}}$.

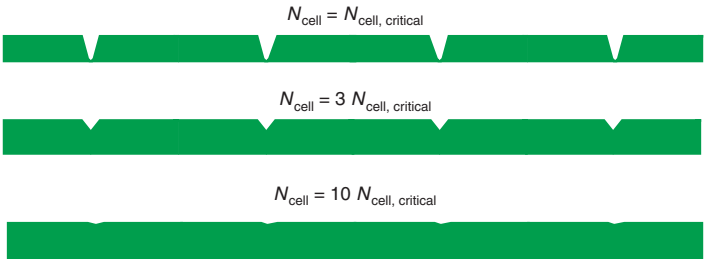

Figure 3. Toy Models. Correlation functions $g(\mathbf{r}_{12})$ are shown for three values of N_{cell}. The cusp depth becomes deeper with decreasing N_{cell}. At $N_{\text{cell,critical}}$ the values of $g(\mathbf{r}_{12}) \to 0$ at each $\mathbf{r}_{12} = 0$ modulo $\mathbf{R}_{12_j}$.

7. QM protocol, Wannier states, boundary conditions, and fluctuations

Wave equation,wave function quantum mechanics is a protocol that permits calculation of stationary states and associated energies for a defined environment. To match reality, various symmetry constraints must be applied so as to restrict the set of allowed wave functions. Many-body wave functions must comply with the Pauli exclusion principle and coordinate exchange symmetry. If the self-interaction between members of a coherent pair is to be modeled, the protocol must make use of a transformation from configuration coordinates to center-of-mass,separation coordinates. There has been an ambiguity in the rules governing this transformation. This paper tests the case where that the transformation expresses double Bloch symmetry.

The assumption that Double Bloch symmetry applies is supported by arguments based on using a Wannier states representation of a stationary state Bloch function [9]. A single-particle Bloch state is expressed as a sum over transiently occupied Wannier states, in each of which a whole particle occupies a single potential well for an unspecified time. A single Wannier state is not a stationary state and breaks periodic symmetry. The Bloch stationary state equals the symmetric sum over all the single-particle Bloch states, in accord with Anderson's symmetry principle [10]. When

two deuterons occupy a set of Wannier states, each deuteron is randomly placed in one of the N_{cell} unit cells. There is a $1/N_{\text{cell}}$ chance that both deuterons will end up in the same unit cell. Since there is no contribution to the Coulomb repulsion potential when the dressed deuterons are in different cells, the effective strength of the Coulomb repulsion is $e^2/(|r_{12}|N_{\text{cell}})$, as deduced by summing over the N_{cell} unit cells. This repulsion potential is the same as calculated using a double Bloch symmetry 2-body wave function.

The time-independent correlation functions $g(\mathbf{r}_{12})$ shown in Fig. 2 have discontinuities in momentum at N_{cell} cusp points in $\{\mathbf{r}_{12}\}$. At each of these points, the kinetic energy $\rightarrow \infty$ at a rate that exactly cancels the singularity in potential energy $e^2/(|\mathbf{r}_{12}|N_{\text{cell}})$. The magnitude and number of momentum discontinuities at the N_{cell} discontinuities is a boundary condition imposed on the 2-body wave function. The boundary condition in $\{\mathbf{r}_{12}\}$ complements the boundary conditions in $\{\mathbf{r}_{\text{cm}}\}$, which define the deuteron containment volume and the multiplicity and shape of potential wells in $\{\mathbf{r}_{\text{cm}}\}$.

In the Bloch picture, the fraction of charge located within any single unit cell is not a precisely measurable quantity. It is subject to quantum fluctuations about an expectation value. This behavior is the same as that described by Greiner *et al.* [11] for a low density set of Bose atoms in an optical lattice. Coordinate-entangled dressed deuterons in a metal lattice may share some properties with Bose atom condensates in an optical lattice.

8. Relevance to cold fusion

It has been widely assumed that the conventional picture of a "Coulomb Barrier", as formulated in scattering theory, should be relevant to Pons and Fleischmann "Cold Fusion". However, we now know that the Pons and Fleischmann claims do not mimic conventional fusion. Cold fusion reactions are not a result of the kinetic collision between two deuterons, and do not involve asymptotic plane wave scattering theory, such as leads to Gamow factors [8]. Instead it involves perturbative interactions between nuclear states formed from protons, neutrons, and resonant groupings thereof, like alpha particles and di-neutrons, as modeled by Wheeler [12]. The interactions between these nuclear components involve continuous potentials that are defined over the full range of distance scales, from subnuclear, through nuclear, through atomic, through the macroscopic dimension scales of metal crystals. Although the nuclear force potentials are confined to nuclear dimension, the electromagnetic interaction potential extends over the full range of length scales where interaction can occur. Furthermore, wave function coherence, expressed as an ordering of wave function phases over macroscopic distances, must be applied to the wave functions of the interacting nuclei.

Cold fusion viewed as a variant of $D^+ + D^+ \rightarrow {}^4He^{++} + \gamma$ takes place without radiation. It occurs rarely because the initial state D's are required to "be prepared" and "entangled" in a particular way. When additional D atoms are forced into a fully loaded PdD lattice, appreciable $D^+ - D^+$ overlap can occur at many different locations, simultaneously, without appreciable D^+ charge accumulation at any particular location. [13] These delocalized deuterons are "Bloch state" deuterons. At large $\mathbf{r}$ their asymptotic form is a Bloch function and not a plane wave. Although this paper does not explicitly deal with problems associated with energy release and dissipation, the Bloch wave function form provides a useful picture for understanding how, in a periodic solid, the conventional "Coulomb Barrier" can be altered through long-range coherence in a way that potentially leads to nuclear reaction [13,14]. The model accomplishes this by replacing the problem of "Overcoming the Coulomb Barrier" with an alternative energy minimization problem.

References

[1] Footnote: The conventional dd fusion reactions (d + d $\rightarrow {}^3H$ + p and d + d ${}^3He$ + n) are computed using Gamow factors.
[2] J. S. Schwinger, Quote from lecture at U. Gourgogne (1990) in *Climbing the Mountain, The Scientific Biography of Julian Schwinger*, by authors J. Mehra, K.A. Milton (Oxford University Press, New York, 2000), p. 554.
[3] F. Seitz, *The Modern Theory of Solids* (McGraw-Hill, New York, 1940), pp. 231–234.

[4] E. A. Hylleraas, Neue Berechnung der Energies des Heliums im Grundzustande, sowie des teifsten von Ortho-Helium, *Zeit. f. Phys.* **65** (1929) 347–366.
[5] T. A. Chubb, S. R. Chubb, Cold fusion as an interaction between ion band states, *Fusion Technol*. **20** (1991) 93–99.
[6] A. J. Leggett, G. Baym, Exact upper bound on barrier penetration probabilities in many-body system: application to 'Cold Fusion', *Phys. Rev. Lett*. **63** (1989) 191–194.
[7] H. Fujita, Studies of atom clusters by ultra-high voltage electron microscopy, *Materials Transactions, JIM* **35** (1994) 563–575.
[8] L. I. Schiff, *Quantum Mechanics* (McGraw-Hill, New York, 1955), pp. 91,117.
[9] T. A. Chubb, S. R. Chubb, Radiationless cold fusion: why small 'Crystals' are better, N_{cell} requirement, and energy transfer to lattice (*Proc. ICCF 6*, 1996), pp. 417–424 .
[10] P. W. Anderson, More is different, *Science* **177** (1972) 393–398.
[11] M. Greiner, O. Mandel, T. Esslinger, T. W. Hansch, I. Bloch, Quantum phase transition from a superfluid to a Mott insulator in a gas of ultracold atoms, *Nature* 4**15**(2002) 39–44.
[12] J. A. Wheeler, On the mathematical description of light nuclei by the method of resonating group structure, *Phys. Rev.* **52** (1937) 1107–1122.
[13] S. R. Chubb, Nuts and Bolts of the Ion Band State Theory (www.lenr-canr.org/acrobat/, file= "ChubbSRnutsandbol.pdf", 2004). S. R. Chubb, "An Overview of Cold Fusion Theory", in "THERMAL AND NUCLEAR ASPECTS OF THE Pd/D_2O SYSTEM", S. Szpak and P. A. Mosier-Boss, Editors, *SSC Technical Report 1862* (SPAWAR Systems Center, San Diego, 2002) pp. 91–111.
[14] P. L. Hagelstein, A Unified Model for Anomalies in Metal Deuterides, in *Proc. ICCF 9*, CONDENSED MATTER NUCLEAR SCIENCE", Xing, Z. Li, Editor (Tsinghua Univ. Press, Beijing, 2003), pp. 121–134.